ChemComm

# Interfacial Processes in Electrochemical Energy Systems



| Journal: | *ChemComm* |
|---|---|
| Manuscript ID | CC-FEA-03-2021-001703.R1 |
| Article Type: | Feature Article |
| | |

ARTICLE

# Interfacial Processes in Electrochemical Energy Systems

Maoyu Wang,[a] Zhenxing Feng*[a]

Electrochemical energy systems such as batteries, water electrolyzers, and fuel cells are considered as the promising and sustainable energy storage and conversion devices due to their high energy densities and zero or negative carbon dioxide emission. However, their widespread applications are hindered by many technical challenges, such as the low efficiency and poor long-term cyclability, which are mostly affected by the changes at the reactant/electrode/electrolyte interfaces. These interfacial processes involve the ion/electron transfer, molecular/ion adsorption/desorption, and the complex interface restructuring, which leads to irreversible modifications to the electrodes and the electrolyte. The understanding of the interfacial processes is thus crucial to provide strategies for solving those problems. In this review, we will discuss different interfacial processes at three representative interfaces, namely solid-gas, solid-liquid, and solid-solid in various electrochemical energy systems, and how they could influence the performance of electrochemical systems.

## Introduction

With the increasing demand for energy resources and awareness of environmental problems, the development of sustainable energy devices has become the main effort in recent decades.[8-10] Electrochemical energy systems (EESs) such as batteries，fuel cells ， and water electrolyzers, have been raising as the promising candidates of the green devices due to their high energy density and low environmental pollutions.[11-13] However, there are still many technical challenges in these EESs, which hampers their large-scale applications.[14, 15] For example, to improve the energy density of current lithium-ion batteries (LIBs), the use of lithium metal as the anode is necessary, but the dendrite formation at the anode-electrolyte interface is a severe problem in batteries that use either solid-state or liquid electrolytes, resulting in safety issues, limited voltage window, and poor cyclability.[17-19] In LIBs, electrode-electrolyte interphase (EEI) is treated as one of the critical elements to improve batteries' performance.[17-19] Luchkin et al. reported that the LIBs performance and cyclability strongly depend on the formation of passivation interphase layers.[21] Also, Suo et al. demonstrated that the EEI could block the electron transfer and only allow ion transfer to expand the voltage window of aqueous batteries.[22] Similarly, hydrogen fuel cells, which convert chemical energy stored in hydrogen to electricity with no carbon emission, and electrolyzers, which split water to produce hydrogen and oxygen, suffer from the sluggish kinetics of oxygen reduction reaction (ORR) and oxygen evolution reaction (OER),[23-26] respectively. The implementation of catalysts at the electrode-electrolyte interfaces in these energy conversion devices is essential to improve the surface reaction kinetics, thus helping achieve high efficiency for the whole system. [27-29] Hong et al. showed that the oxygen adsorption and dissociation on the electrode surface is important for improving the electrocatalyst function.[30] Clearly, all these studies have indicated that the interfaces are critical components and the processes at these interfaces can significantly influence the performance of EESs.

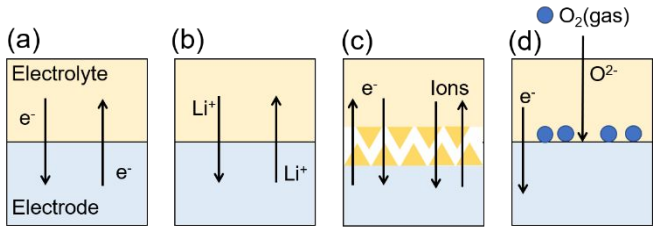


Figure 1: Interfacial processes schematic for (a) electron (charge) transfer (b) ionic transfer (c) surface reconstruction (d) surface adsorption/desorption. The Li ions and oxygen electroreduction reaction is shown as an example.

Therefore, to design next-generation EESs, it is necessary to conduct the fundamental research at these interfaces and understand the connections between the interfacial processes and devices' performance. In this Feature Article, we will go over and summarize current progresses on studies of interfacial processes in different EESs.

There are several different types of interfacial processes which can be categorized based on the effects on interfaces. The simplest one only involves the electron or charge transfer (Figure 1a), which can take place on the electrocatalyst surfaces but may not be desired in most electrode-electrolyte interfaces in EESs, as electron should be only allowed through outside wires. Only ionic transfer is preferred at the electrode-electrolyte interfaces (Figure 1b). For example, Wang et al. reported a new type of aqueous battery electrolyte reacting with Li anode to form a stable EEI, which would limit the electron transfer and allow Li ion transfer to expand the battery voltage window.[31] Different from the electron transfer, ions have a relative large size than electrons, which may cause structure changes at these interfaces. For the intercalation type batteries such as LIBs, the intercalation of $Li^+$ may or may not result in any interfacial modifications.[32] However, such interfaces always change in conversion-type batteries such as lithium-sulfur batteries.[33] The third case involves both electron and ion transfer (Figure 1c), which can lead to significant surface reconstruction at the interface and it is the

most common interfacial process (e.g., the formation of the solid-electrolyte interphase, or SEI).[34-36] The forth case is the surface adsorption/desorption, which is well known in electrochemical systems that involves gas or reaction intermediates such as electrocatalyst surfaces in fuel cells and water electrolyzers.[37-39] Similar to the ion transfer reaction, the surface adsorption/desorption may result in surface reconstruction. For example, Wygant et al. pointed out that most transition metal carbide, pnictide, and chalcogenide such as FeS, CoS, and NiS would undergo surface reconstruction when adsorbing oxygen ions during OER, but some transition metal chalcogenide such as NiSe may not experience surface structure change.[40] In this Feature Article, we will go over the recent progresses of solid-gas, solid-liquid, and solid-solid interfaces in different electrochemical energy systems to illustrate corresponding interfacial processes. We will also briefly discuss related characterization techniques, particularly *in-situ* and *operando*, which are suitable to probe the complex changes.

## Solid-Gas Interface

Solid-gas interface (SGI) commonly exists in chemical reactions, particularly in heterogenous catalysis, where the molecules are absorbed on catalyst surfaces and subsequently react and desorb. Research in surface science has been diversely developed by studying the restructuring and changes at the SGI in catalysis. In addition to understand such processes in either bulk powders or nanoparticles,[41-47] single crystal and thin films are widely used as the model systems to study chemical reactions at the SGI through numerous surface-sensitive techniques (e.g., X-ray, electron microscopy etc.), with great insights obtained.[48-59] In electrochemical devices, such interfaces can be found in gas-breathing components. For example, fuel cell cathode and anode that involve gas adsorption and charge transfer are one type of SGI. The metal-air batteries also need to accommodate the air or oxygen diffusion through the corresponding electrode, thus forming SGI. One of the best examples on SGI could be the anode and cathode of solid oxide fuel cells (SOFCs),[60-62] which is operated at elevated temperature (500 $^{o}$C – 1000 $^{o}$C) to react with hydrogen and oxygen, respectively, and is a potential alternative to conventional fire-power plants for electricity generation owing to SOFCs' high efficiency and low carbon emission.[60, 63, 64] A typical SOFCs process involves the electrochemical reduction of oxygen molecules over the cathode to oxygen ions, the diffusion of oxygen ions through the electrolyte and then to the anode for the reaction with hydrogen. The sluggish ORR kinetics at the cathode and poor oxygen ionic conductivity are two major issues that affect the performance of SOFCs and hinder their large-scale utilization.[60, 63, 64] Researchers have found that if the cathode thickness is less than the critical thickness ($L_c$) that is defined by the ratio of diffusion coefficient ($D$) and surface exchange coefficient ($k$),[65, 66] the rate limiting step is ORR at the surfaces, otherwise the bulk diffusion limits the whole reaction. Clearly the two processes are associated with the SGI, and Figure 2 illustrates three scenarios which can be further categorized as dual phase boundary (DPB) and triple phase boundary (TPB).[67] The following discussions will be focused on the cathode interfaces of SOFCs as examples.

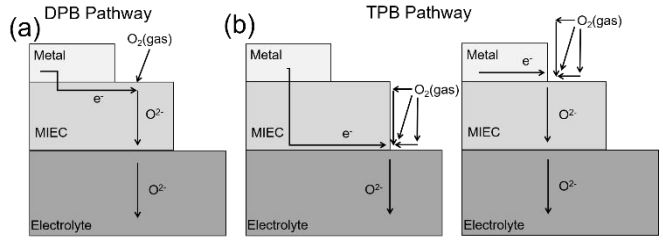


Figure 2: A schematic of reaction pathways involving (a) DPB and (b) TPB through metal, MIEC and electrolyte. The ORR is shown as an example

In DPB, the oxygen gases interact with solid cathode or catalyst interfaces and go through the following processes: the oxygen molecule directly absorbed on the mixed ionic electron conductor (MIEC) and disassociate to oxygen atoms or is directly reduced to oxygen ions, and then the oxygen ions diffuse through the electrolyte to the anode (Figure 2a).[67] Those adsorption and diffusion may lead to some surface structure modification or degradation. The oxygen adsorption and dissociation can be facilitated by either the cathode itself or additionally added catalyst materials, and the surface restructuring or degradation directly influence both performance and durability of SOFCs. Therefore, controlling the undesired side reaction and inhibiting the surface degradation at the SGI is one promising way to improve the performance of SOFCs. An effective means is to modify the surface composition or coat/decorate a thin layer that prevents the restructuring. For example, Pang et al. found that optimization of surface composition of $La_{0.5}Ba_{0.5}CoO_x$ by creating Ba-deficiency can suppress the formation of the segregation layer, decrease the oxide ions diffusion barrier, and stabilize the crystal structure for the better ORR durability and activity.[68] Moreover, Yang et al. reported that $SrFe_{0.85}Ti_{0.1}Ni_{0.05}O_x$ decorated with NiO nanoparticles demonstrated the better ORR activity than the benchmark cobalt based $Ba_{0.5}Sr_{0.5}Co_{0.8}Fe_{0.2}O_x$, and those NiO was treated as the important components to enhance ORR performance.[69] Li et al. also demonstrated that the $Co_3O_4$ decorated $LaSrFeO_3$ surface will improve the surface ORR kinetics by changing the charge-transfer processes and increasing the surface oxygen exchange coefficient. Note that not all surface layers can prevent the surface restructuring and/or enhance the ORR activities. Shao-Horn group has showed that the surface decoration of $La_{0.8}Sr_{0.2}CoO_{3-\delta}$ with Sr composition (e.g., SrO) can enhance the surface exchange coefficient and ORR activity, while "La"- and "Co"-decorations lead to no change of ORR.[70] Those studies have successfully confirmed that the surface composition and structure are important for ORR kinetics, and similar strategies have been applied in battery research for surface coating on cathode materials to improve the stability and performance,[71] which will be illustrated more later. However, these studies have not provided deep insights on how surface composition or structure would change the reaction kinetics. Besides reports showing the effectiveness of surface coating on DPB for the improvement on solid-gas interfacial processes, it is more important to figure out the physical origins for such enhancements or changes at the SGI.

To better understand this interfacial phenomenon in DPB, Rupp et al. used the real-time *in-situ* electrochemical impedance spectroscopy (EIS) to monitor the oxygen reduction processes during surface modification of $LaSrCoO_x$ (LSC) cathode, which shows the excellent activity for ORR but poor durablity.[14] To find out the potential reason causing those degradations, they measured the surface exchange resistance and coefficient when growing the LSC with tiny amount of

SrO by pulsed laser deposition.[14] They found that SrO would lead to the deactivation of the LSC and the Co adding will (re-)active the LSC.[14] The surface exchange resistance would increase and the surface exchange coefficient would decrease with more Sr decorated surface, but the Co showed the opposite trend to the Sr.[14] Moreover, the La decorated surface would not affect the surface exchange resistance and coefficient a lot.[14] The results indicates that Co atoms is the active sites for ORR, and the decomposition of LSC will lose Co atoms on the surface, which resulted in the deactivation of LSC.[14] This finding seems to contradict other results which show the Sr enrichment in surface actually benefits the surface ORR.[70, 72, 73] To clarify these differences, Adler group utilizes linear and non-linear impedance analysis on several gas-solid interfaces of LSC thin films including $La_{0.8}Sr_{0.2}CoO_{3-\delta}$ and $La_{0.6}Sr_{0.4}CoO_{3-\delta}$ under different partial oxygen pressure (Figure 3a-3c),[1, 74] and revealed that these surfaces still obey a dissociative adsorption rate law despite substantial changes in local properties. The enhancement caused by surface decoration or additional layer is primarily due to differences in local thermodynamic properties rather than a shift in the reaction mechanism, which clarifies some debates in literature arguing the unique properties of surface layers. Besides electrochemical methods for the mechanistic studies, several synchrotron X-ray characterizations have also been extensively applied to study gas-solid interfaces in electrochemical devices, particularly SOFCs. Considering the surface sensitivity, X-ray photoelectron spectroscopy (XPS), especially ambient-pressure XPS (AP-XPS), is the primary choice for *in-situ* investigations. These *in-situ* characterizations were performed under various oxygen partial pressures with heating and applied voltages, truly mimicking the real operation conditions for electrochemical devices. Such studies have successfully coupled surface composition changes with heating (Figure 3d) and applied voltages.[4, 73, 75] The reversible surface compositional changes under operation conditions are correlated to role of corresponding element in promoting the ORR and contributes to the stability of the gas-solid interfaces for long term run,[73, 75] while some irreversible composition and structural changes at the initial cycles are believed to the activation processes of SGI that induces the local properties for subsequent ORR activity enhancement.[5] These *in-situ* studies at atomic-scale correlate the Sr composition changes with the enhanced ORR activity in thin film cathodes of SOFCs: the Sr enrichment in crystal lattice (so-called coherent Sr) is beneficial for oxygen incorporation thus ORR and incoherent Sr particles on thin film surfaces are detrimental to solid-gas processes. In addition to experimental characterizations, the theoretical calculations are also critical to connect structural and composition changes with the performance of electrochemical devices, especially helpful to reveal the charge-transfer processes and adsorption power of molecules at SGI with respective to the surface oxygen exchange.[76] In theory, one can selectively study one factor's influence on SGI. For example, Xu et al. carried out a theoretical simulation to investigate the adsorption and dissociation of oxygen on the different $Co_3O_4$ planes, which could guide to find a suitable crystal orientation for the best ORR kinetics.[77] They pointed out that the $Co_3O_4$ (001) plane has the smallest oxygen adsorption (-1.905 eV) and dissociation energies (1.69eV) comparing with (110) and (111) plane. Based on the guiding from the theoretical simulation, the $Co_3O_4$ nano-cubes with (001) planes are exposed at the surface and applied in the cathode of

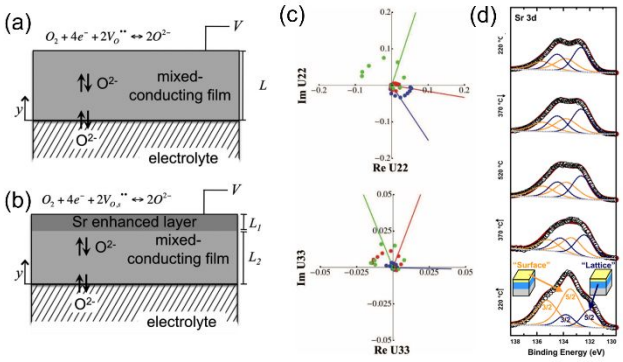


Figure 3: Schematic illustrating two possible distributions of Sr dopant within the LSC thin film: (a) uniform cation distribution; and (b) Two-layer model in which the Sr/La ratio is enhanced within a layer of thickness of L1 near the gas-exposed surface.[1] (c) Measured 2nd and 3rd order harmonic response coefficients $U_{2,2}$ and $U_{3,3}$ for the 45 nm film tested at 520°C and $p_{O2}$ = 1.0 atm (blue), 0.1 atm (red) and 0.01 atm (green). (d) Sr 3d AP-XPS spectra of 90 nm LSC collected during the first heating.[5]

SOFCs,[77] showing the best ORR performance among different crystal orientations.

Comparing with relatively simple reaction process in DPB, the TPB involves more complex interfacial processes: the oxygen molecules are adsorbed and reduced on the interface of solid electrocatalyst and electrolyte, which is the solid-solid-gas interface (SSGI) (Figure 2b).[67] Like DPB, the surface composition and microstructure affect oxygen adsorption and dissociation, thus determining the fuel cell performance and cyclability. Chen et al. demonstrated a conformal $CoO_x$ layer deposited on $(La_{1-x}Sr_x)MnO_3$ (LSM) and yttria stabilized zirconia (YSZ) backbone would improve the ORR kinetics[78]. Previously, surface $CoO_x$ layer was deposited on the cathode or catalyst surface (e.g., DPB) only to improve the catalytic activity, but here they introduced it on both cathode electrocatalyst and electrolyte, which formed a newly added triple phase boundary.[78] Those new TBP, which involves solid electrode-electrolyte interface different from DPB, reduced the polarization resistance dramatically and accelerated the oxygen diffusion to promote ORR kinetics.[78] Studies have also suggested that the length, density, width, connection of TPB are an important microstructural metric to assess the performance and durability of SOFCs,[79-84] as these parameters can affect the available active sites for ORR. For instances, the TBP with greater length has more available reaction sites. Cai et al. reported a simple laser micro-processing to improve the SOFCs performance by changing the TBP structure with extended length. From their scanning electron microscopy (SEM) images, they showed that the laser micro-processing could create the dimples and small cracks, improving the connecting between electrolyte and electrocatalyst and the interfacial area. Those changes resulted in remarkably decreasing of both ohmic and polarization resistance, subsequently increasing the cell power density up to 58%.[85] Similarly Jeong et al. demonstrated that sputtered ultrathin platinum-gadolinium doped ceria (GDC) cermet interlayer on the cathode side of electrolyte increased the triple phase boundary density and enhanced the reaction kinetics for ORR.[86] Those examples proves that the microstructures of TPB (e.g., density and length) are strongly linked to TPB properties. Based on such conclusion, Zhang et al. used a three-dimensional (3D) microstructure simulation to predict the

influence of the microstructure (volume fractions of constituents, particle size, shape, and the thickness ) of TPB on SOFCs' performance.[84] The simulations suggested that the greater porosity above 10% and below 35% of the TPB could lead to the best stability and performance. Both constituents (electrolyte and electrode) have volume fraction above 30% would have more than 87% active TPB. Their results also showed that reducing the thickness of a composite cathode could improve the TPB activity and using non-equiaxed particles increases connectivity and thus reduces the percolation threshold.[84] Besides the cathode side, the TPB is also important at the anode side. Vivet et al reported a 3D imaging study of Ni-YSZ anode by using the focused ion beam SEM (FIB-SEM) tomography. They reconstructed the 3D microstructure from FIB-SEM data to visualize the interfacial features such as surface area and TPB length, and figured out that the optimized NiO composition in Ni-YSZ would result in the largest interfacial surface area and TPB length.[87] Although FIB-SEM provides direct images of SSGI, most measurements are destructive, thus hard for *in-situ* experiments. Other non-destructive methods such as synchrotron X-ray tomography were then used to characterize the TPB segmentation,[82] providing direct evidence of the changes of TPB and correlated that with the fuel cell performance.

It is noted that TPB does not only refer to the electrode-electrolyte-gas interface, but it can also be the electrode-electrode-gas interfaces. In SOFCs, there is a long-time debate about the origin of the superior ORR activity at the heterostructured cathode-cathode-gas TPB interface such as $(La_{1-y}Sr_y)_2CoO_{4+\delta}/La_{1-x}Sr_xCoO_{3-\delta}$ ($LSC_{214}/LSC_{113}$) where either oxygen atoms or oxygen ions react and further diffuse to electrolyte, exhibiting several order of magnitude higher surface oxygen exchange coefficients than that at the pure thin film (e.g., $La_{1-x}Sr_xCoO_{3-\delta}$) or bulk powder cathode-gas DPB. It is hypothesized that the interfacial composition and structure affect the ORR activity. By creating a cross-section of such heterostructured thin film, Yan et al. used the scanning tunnelling microscopy/spectroscopy (STM/STS) to study the electronic structure of the TPB under elevated temperatures.[88] They found $LSC_{214}$ was electronically activated at 200-300 °C and attributed this activation to the strongly anisotropic oxygen incorporation kinetics at the TPB which leads to higher ORR activity. However, the cross-section of the heterostructure with a slope cut may not represent the true TPB. To probe the interfacial structure, advanced techniques with good penetrating power are needed. Synchrotron X-ray with energy higher than 5 keV (hard X-ray) is suitable to study the buried interfaces. Feng et al. used surface X-ray scattering (SXRD) together with coherent Bragg rod analysis (COBRA) to exam and compare the $La_{1-x}Sr_xCoO_{3-\delta}$ cathode-gas DPB and $(La_{1-y}Sr_y)_2CoO_{4+\delta}/La_{1-x}Sr_xCoO_{3-\delta}$ heterostructure TPB.[4, 89] They found in both cases there are significant Sr enrichment at the DPB surface and TPB interface (Figure 4a), which leads to high oxygen vacancy concentration due to the charge neutrality. Such oxygen deficiency is beneficial for ORR as not only oxygen vacancy can facilitate the oxygen absorption and diffusion (Figure 4b), but also elevate the oxygen *p*-band center, which is treated as the design parameter to guide the discovery of highly active cathode and electrocatalysts for numerous electrochemical reactions (Figure 4c).[90-93] Following Feng's research, Chen et al. applied a combination of synchrotron X-ray spectroscopy (i.e., hard X-ray photoelectron spectroscopy) with high resolution

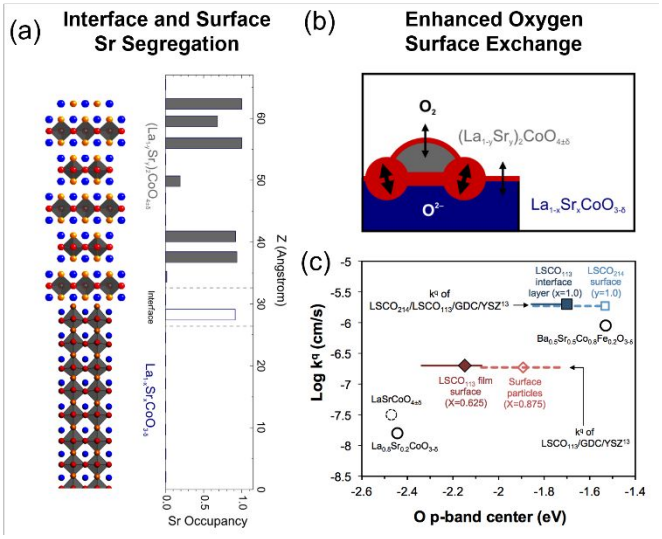


Figure 4: (a) Model $(La_{1-y}Sr_y)_2CoO_{4+\delta}/La_{1-x}Sr_xCoO_{3-\delta}$ heterostructure thin film interfaces and layer-by-layer Sr distribution obtained from SXRD and COBRA analysis. (b) The interface and surface Sr segregation in lattice leads to the enhanced oxygen surface exchange rate at the SSGI (c) surface exchange coefficients $k^q$ or k* vs. the calculated O 2p band centers (relative to the Fermi level) calculated for bulk unit cells. Detailed can be found in reference.[4]

XRD (HRXRD) to study various heterostructure TPB and arrived the similar conclusion that the oxygen defect chemistry of these transition metal oxides was strongly impacted by the presence of interfaces and the properties of the adjacent phases.[94]

## Solid-Liquid Interface

Solid-liquid interface (SLI) is another important component in many electrochemical energy systems, particularly, for electrocatalysts in energy conversion devices and electrode-electrolyte interfaces in liquid electrolyte-based batteries. Similar to the SGI, there are various interfacial processes occurring at SLI, including electrodeposition, reactions, transformations and restructuring. The liquid medium allows the transportation of both gases and ions, adding additional complicity compared to SGI. In addition, SLI maintains good flexibility to adapt to structural deformation during different interfacial processes. Therefore, the complicated but important SLI attracts great scientific attentions from electrochemistry community to study the structure-property relationship in electrochemical energy devices.

The charge transfer is one major process at the SLI and is commonly found in reactions involving electrocatalysts, which typically leads to the chemical adsorption/desorption of molecules on surface and/or the subsequent surface reconstruction. In the past decades, efforts have been made to understand the molecular interactions with electrocatalysts and related influences on catalytic properties.[34, 95-99] The *d*-band center theory proposed by Norskov has paved the foundation in catalysis to link the adsorptive power of catalysts to their activity.[100] For example, they used the density functional theory (DFT) to figure out that the stable adsorbed oxygen and hydroxyl due to proton/electron transfer at the interface of the solid electrocatalysts and liquid electrolytes are the origin of the overpotential of ORR.[101] Such studies provide guidance for rational

modification of catalysts to achieve the desired activity and selectivity. Based on this theory, a lot of follow up work have been done for numerous electrochemical reactions. Duan et al. applied DFT to predict that the transition metal modified Pt surface would have weaken the adsorption strength of hydroxyl/oxygen and then can improve the ORR performance.[102] By alloying with transition metals, Greely et al. tuned the adsorptive power of Pt at optimum and successfully suggested $Pt_3Ni$ electrocatalyst that is cheaper than Pt but has higher ORR activity.[103] With this theoretical guidance,[104] scientists have design special nanostructure (e.g., $Pt_3Ni$ nanoframes) with superior ORR activity and stability (i.e., no decay for more than 10,000 cycles' use).

In addition to theoretical studies, experimentally surface adsorption/desorption concurring with charge-transfer has been found in many cases. Due to the complicity of the interfacial changes at SLI, thin film or single crystal model systems are usually used to provide well-defined, singly orientated surfaces. Taking $RuO_2$ as an example, it is a well-known, highly active electrocatalysts for OER but its surface changes due to the interactions with molecules and reaction intermediates are largely unknown. Shao-Horn group combined *in-situ* surface-sensitive X-ray scattering techniques with DFT to study the (110)-orientated $RuO_2$ single crystal surface at the SLI in acidic condition as a function of the applied voltage.[7] The X-ray scattering measurements showed that (01L) and (10L) rods are the oxygen atoms sensitive rods corresponding to changes in surface adsorbed oxygen species, and (00L) rods is predominantly dependent on Ru atom position (Figure 5).[7] When increasing the potential, the intensity of (00L) rods did not change, which indicates the position of surface Ru did not move in OER (Figure 5c).[7] However, the scattering intensity variation from (01L) and (10L) rods suggests interfacial structural changes due to the adsorbed oxygen species with applied potential (Figure 5a and 5b).[7] The surface structure obtained from the fitting of X-ray scattering data provides the quantitative information of the Ru-O bonding lengths (Figure 5d-5k).[7] With further help from DFT to examine the energetics of the surface structure, they demonstrated that the deprotonation of the hydroxyl group would form a stabilize -OO group to limit the whole OER kinetics.[7] Later, the same group carried out a more comprehensive investigation of the oxygen/hydroxyl adsorption/desorption on the $RuO_2$ surface with four different orientations, namely (101), (110), (001), and (100), using a combination of the AP-XPS, *in-situ* SXRD, and DFT.[105] They found that different surface orientations can have different degrees of influence on the adsorptive powers for reaction intermediates and can be used to tune catalysts' OER activity by varying the density of active sites.[105] The two cases are few experimental studies that directly reveal the molecular adsorption/desorption caused by charge-transfer in reaction,[104, 106, 107] mainly due to minor or negligible local structural changes at SLI from molecule adsorption/desorption. It is more plausible to monitor the electronic structure changes at SLI using spectroscopy, as charge-transfer can modify the electron configurations.[108-110]

Strong interfacial restructuring can also be induced by the charge-transfer process at SLI and is also common in electrocatalysis.[111-115, 116] The restructuring can be either reversible or irreversible. The former is generally good for electrocatalysts' long-term use and has been reported in many studies,[115, 117-123] while the latter is believed to be detrimental to catalysts' performance. In most cases, the surface of the electrocatalysts become amorphous and loses their original activity. Experiments have demonstrated that perovskite $Ba_{0.5}Sr_{0.5}Co_{0.8}Fe_{0.2}O_{3-\delta}$ (BSCF82) is not only highly active as the cathode in SOFCs to promote reactions at SGI, but also a good electrocatalyst for OER in alkaline solutions. However, it is not stable in reaction.[124] To study the deactivation mechanism, May et al. applied high resolution transmission electron microscopy (HRTEM) to compare the surface of the BSCF82 before and after the reaction. They found that the surface amorphization caused by reduced surface concentration of Ba and Sr ions in charge-transfer catalytic process is the reason that degrades the OER activities.[125] However, not all amorphization leads to the activity loss for electrocatalysts. $SrIrO_3$, a recently discovered material with ~3 order of magnitude higher in OER activity compared to the commercial standard $IrO_2$ in acidic condition, exhibits better and better performance during cycling.[126] It was originally attributed to the Sr leaching and the formation of $IrO_2/SrIrO_3$ heterostructure. The follow-up mechanistic study, which combined surface-sensitive scattering as well as spectroscopy and DFT, reveals that there are actually two changes of $SrIrO_3$ during the reaction.[127] The Sr leaching results in the Sr-deficient $Sr_yIrO_x$, and at the same time the top surface (~2.4 nm) turns into amorphous structure. This special interfacial restructuring

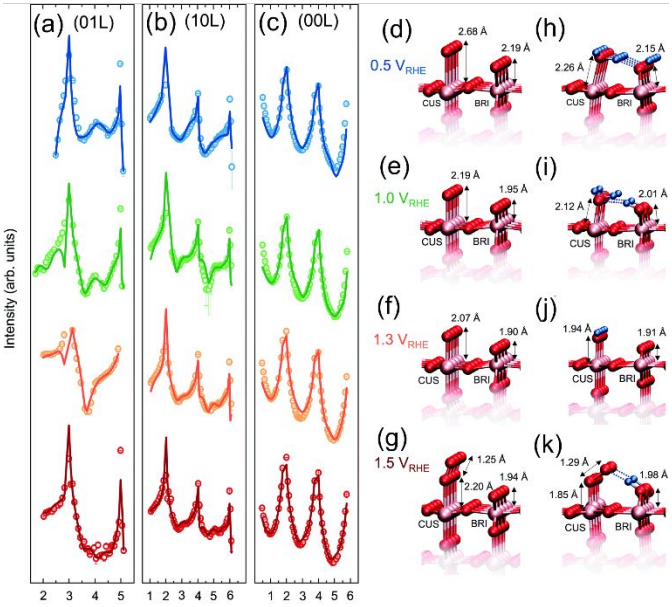


Figure 5: (a) (01L) (b) (10L) and (v) (00L) rods measured at the four different potentials, 0.5 V, 1.0 V, 1.3 V and 1.5 V as indicated. All voltages here are versus reversible hydrogen electrode (RHE). The experimentally measured intensities are shown as open points and the best-fit results from the fitting process are shown as solid lines of the corresponding color. Ball and stick models for the best-fit structures obtained for the (d) 0.5 V, (e) 1.0 V, (f) 1.3 V and (g) 1.5 V crystal truncation rod data. Maximum experimental uncertainty in bond lengths is 0.06 Å. Most stable adsorbate configuration obtained from DFT calculations at (h) 0.5 V and (i) 1.0 V. The $Ru_{CUS}$–O bond length is the average value of the $Ru_{CUS}$–$H_2O$ (2.17 Å) and $Ru_{CUS}$–OH (2.07) Å and the $Ru_{BRI}$–O bond length is an average value of the $Ru_{BRI}$–OH (2.10 Å) and $Ru_{BRI}$–O (1.92 Å) at (j) 1.3 V and (k) 1.5 V. The $Ru_{CUS}$–O bond length is the average value of the $Ru_{CUS}$–O (1.73 Å) and $Ru_{CUS}$–OO (1.96) Å and the $Ru_{BRI}$–O bond length is an average value of the $Ru_{BRI}$–OH (2.07 Å) and RuBRI–O (1.89 Å). Pink, red and blue spheres represent Ru, O and H atoms respectively. Bond lengths between surface Ru and adsorbed O species are labeled. ($Ru_{CUS}$: a coordinately unsaturated Ru site bound to five O atoms; $Ru_{BRI}$: a bridge Ru site bound to six O atoms)[7]

is initiated by the lattice oxygen redox and is beneficial for OER due to the coupled ionic diffusions.[127] Instead of forming special heterostructure, the highly disordered Ir octahedral network with Ir square-planar motif in the amorphous layer is confirmed by DFT to be the active center of the electrocatalyst.[127]

We want to emphasize that the irreversible restructuring at SLI other than amorphization could also be good for electrocatalysts at the SLI. Several works have shown that there could be an activation change in electrocatalysts at the very beginning of the reaction. In a study of single Ru atom anchored on the transition metal double layer hydroxide as electrocatalyst for OER, Li et al. identified Ru-O-M (Fe, Co, Ni, and Cu) motifs on the electrocatalyst surface after synthesis and detected the shortening of the bond length after the first cycling. They suggest that Ru-O-M configuration changes the electron distribution and promotes electron transfer from M to Ru.[128] Those electron transfers would not only benefit the oxygen adsorption confirmed by DFT but also prevent the Ru being oxidized to higher oxidization state and dissolving in the electrode, consequently increasing the electrochemical stability.[128] Similar situation was found in another study using nickel-iron layered double hydroxide as the OER electrocatalyst. Interestingly, the Ni goes through reversible oxidation state changes in the reaction while Fe experiences an irreversible restructuring initially. The reversible change of Ni contributes to the regulation of the local structure and makes high-valent metal sites stable at low overpotentials.[129] The irreversible change of Fe enables a special $Fe^{4+}$ state that serves as the active site of OER and contributes to high activity of the layered double hydroxide.[129]

All these examples shown above suggest that the interfacial restructuring is a complicate process at SLI. To better track such changes with deep understanding, *in-situ* and *operando* characterizations such as X-ray absorption spectroscopy (XAS) are necessary.[2, 128, 130, 131] One good example is from our study on high-loading atomically dispersed Ir atoms anchored on the amorphous CoO surface using *in-situ* XAS.[2] Although XAS is a bulk-sensitive technique, the material of interest is on the surface so the measurements on the material becomes surface-sensitive. As shown in Figure 6a, the X-ray absorption near edge structure (XANES)

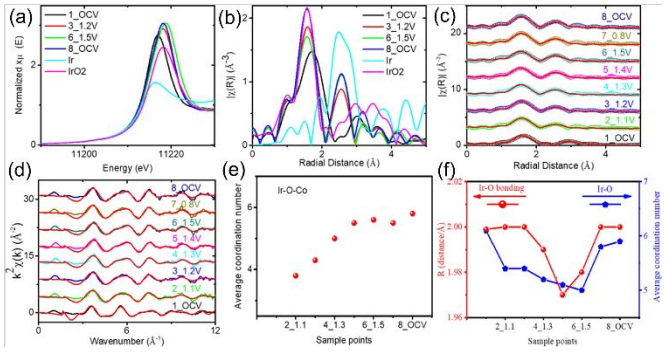


Figure 6: XAS results of $Ir_1Co_{13.3}O_{20.1}$. In situ Ir L-edge (a) XANES and (b) EXAFS under various reaction potentials. Fourier transfer EXAFS fitting of in situ Ir during the reaction: (c) R-space and (d) k-space. The average coordination number of Ir–O–Co during the OER (e). The Ir-O bonding distance and the average coordination number of Ir–O during the OER (f).[2]

pointed out that the Ir would be oxidized with increasing applied potential and reduced with decreased applied potential.[2] The extended X-ray absorption fine structure (EXAFS) indicated that the surface anchored Ir would move towards to the CoO bulk to form a strong Ir-O-Co bond (Figure 6b). In addition, the EXAFS also shown the increase and decrease of Ir-O coordination number (Figure 6c-6e), which stands for the oxygen species adsorption and desorption, respectively.[2] Such reversible restructuring of Ir-O-Co bonding, as discussed above, would change the electron distribution around Ir and Co, thus benefiting the oxygen adsorption/desorption during the charge-transfer process at SLI.[2] Furthermore, a lot of bulk-sensitive techniques can be tuned surface-sensitive when operating at grazing-incidence angle.[132, 133] For example, Lee et al. carried out the *in-situ* grazing incidence XAS (GIXAS) and XRD (GIXRD) to study the polycrystalline Cu thin film surface during the electrochemical carbon dioxide reduction reaction (CO2RR).[133] Their results showed that the surface CuO would be reduced to Cu that is the only phase presenting under the CO2RR condition, and the polycrystalline Cu surface would reconstruct toward Cu (100) surface.[133] This is similar to our study on the reconstruction of copper(II) phthalocyanine (CuPc) during CO2RR.[123] We also found the reduction of CuPc to form Cu nanoclusters, but differently our results indicate that those Cu nanoclusters can be reversed back to CuPc once the applied potential is back to the open circle potential, thus CuPc can be reused many times in reaction.[123] The similar processes observed by the two groups with different final products in CO2RR are not contradictive to each other. The difference could be lied in the nucleation and growth condition. In the CuPc case, the size of Cu nanoparticles is too small to have a stable nucleation seed and then decomposes once the potential is reversed, while the Cu thin film could be strongly bonded by the underneath substrate without further change. The two studies also emphasize the importance of advanced *in-situ* characterization techniques for investigating complex interfacial processes in SLI.

Besides the electrocatalysts and/or electrode influence on the SLI, we also want to bring attention to the electrolyte influence on the SLI.[134-140] The pH of the electrolyte is one important parameter affecting the molecular absorption capability at SLI.[135, 137] Li, et al, used the $IrO_x$ as a model system to demonstrate that $IrO_x$ shows 6.5 times higher OER activity in 4.0 M KOH than 0.1 M KOH due to the stronger $OH^-$ adsorption.[136] They further pointed out the adsorption and interaction $OH^-$ would also be affect by using different cation at the same pH.[136] They found that the $Na^+$ would help form a stronger noncovalent interaction with OH than $K^+$ to decrease the interfacial $OH^-$ mobility, which worse the OER performance.[136] In addition, Waegele, et al. recently reviewed the cation effect of the electric double, reaction rates, and selectivity by influencing the SLI.[140] Moreover, the anion would also affect the surface absorption and restricting at SLI.[134, 137] Arminio-Ravelo, et al. studied the SLI by using standard Ir-based nanoparticles in two different acid electrolyte ($H_2SO_4$ and $HClO_4$). They found that the Ir black nanoparticles is likely to be faster oxidized in $H_2SO_4$ than in $HClO_4$ which cause Ir are less active in $H_2SO_4$ than $HClO_4$.[137]

When moving from electrocatalysts to the electrode-electrolyte SLI in liquid-electrolyte-based batteries (LEBs, such as lithium/sodium ion batteries, aqueous batteries, multivalent batteries, and dual-ion batteries), the interfacial processes become more complicated.[141-150] For electrocatalysts, although charge-transfer induced changes such as molecule adsorption/desorption dominate at the SLI, there is little

or no reaction between the electrocatalyst and the electrolyte.[28, 38, 151] However, since both ion and electron transfers take place at the SLI in the LEBs, electrodeposition and interfacial transformation could also be induced in addition to interfacial restructuring discussed in electrocatalyst systems.[99, 152, 153] For example, the well-known SEI in lithium-ion batteries is a product from these complex interfacial processes, which involve the decomposition of the electrolyte, electrodeposition of the reaction products on lithium metal or graphite anode, and interfacial restructuring at the anode side.[154] The studies of SEI have been carried out for a long time but limited progresses have been achieved due to the difficulties to detect the dynamic formation of the thin interfacial layers that contain mostly light elements. Until recent years, with the application of advanced cryo-electron microscopy and synchrotron X-ray scattering,[19, 155-158] researchers can study the SEI, either quasi-*in-situ* at the frozen state or completely *in-situ* and obtain the structural and compositional information at the atomic-scale. These studies have shown that the SEI composes of both crystalline and amorphous structures and contains not only LiF but also LiH. In addition to lithium-ion batteries, SEI is also an important component in other LEBs.[34, 159-161] Ko et al. reported a SEI formed at the anion-derived solid electrode and liquid electrolyte interface, which would decompose or dissolve in the free (or uncoordinated) water molecules but can be retained stably in the water-in-salt electrolyte.[98] This SEI is critical as it can expand the operation voltage window in aqueous batteries and suppress the side hydrogen evolution reaction.[98] Furthermore, Munster, et al found a SEI consist of the degradation products of bis(fluorosulfonylimide) (FSI) salt at high concentration in potassium dual-ion batteries.[152] The SEI formation would suppress the degradation of the solvent during potassium (de)intercalation and reduce the charge transfer resistance.[152]

Comparatively the cathode-electrolyte interphase (CEI) is easier to study. The CEI is formed on the oxide (e.g., $LiCoO_2$) surfaces which can be studied not only on powders using advanced techniques such as cryo-electron microscopy but also on thin film model systems with well-defined surfaces.[162] Lu et al. grew $LiCoO_2$ (LCO) microcrystals on Al substrates and used *in-situ* atomic force microscopy (AFM) to investigate the surface morphology. They found that the LCO would react with liquid electrolyte ($LiPF_6$) and Co will continue dissolving into the electrolyte at higher voltage above 4.2 V.[154] They also found when adding a thin $Al_2O_3$ layer on top of LCO, the reaction between $LiCoO_2$ and $LiPF_6$ can be suppressed.[154] Interestingly $Al_2O_3$ is neither $Li^+$ conducting nor electron conducting. Therefore, a lot of efforts have been focused on understanding how such material can be beneficial for interfacial progresses.[17, 18, 163-165] In particularly, our group developed a facile synthesis protocol via sol-gel method to coat $Al_2O_3$ on commercial LCO surface and investigated the thickness-dependent effects on battery performance.[71] It turned out a very thin layer (50 nm or less) has good mechanical flexibility and does not block $Li^+$ diffusion at the SLI. By employing XAS, we showed that unprotected or incompletely covered LCO would react with the Li ions to form $Li_2O$ and reduce LCO to Co, thus causing the degradation of both electrode and electrolyte.[71] In contrast, a thick $Al_2O_3$ coating would affect the ionic and electronic conductivity, which increases the transportation resistance and decreases the overall battery performance.[71] This surface coating strategies have been successfully applied on cathodes and anodes in batteries to prevent unwanted interfacial reactions at the SLI, and can be extended on other electrode-electrolyte interfaces to improve the interfacial stability.

Besides the formation of interphase at the SLI, ionic diffusion across the interface is another important interfacial process in LEBs. The host structure at the electrode can strongly influence the ionic diffusion at the SLI, as demonstrated by $LiMn_2O_4$ (LMO) cathode that can take up two $Li^+$ at maximum but in commercial battery cell is only cycled with one $Li^+$ to maintain the structure stability.[166] To figure out ways for improving the energy capacity of LMO, Chen et al. used thin film to obtain epitaxially grown LMO. The lattice confined structure enables the capability of LMO to host two $Li^+$ without any phase transition, which is confirmed by *in-situ* and *operando* X-ray reflectivity and XRD under the Li insertion and extraction.[166] They further found that no measurable Mn dissolution/loss during the Li insertion but dramatic Mn loss during the deeper discharge causing by the lattice strain change of LMO, which provides new insights on how to improve the capacity while maintaining stability of LMO.[166] The strategy of using lattice confinement has been applied in multivalent batteries as well. Using MgO substrate to induce strain, high-temperature high-pressure phase of cubic $MgMn_2O_4$ (MMO) has been synthesized at room temperature as the thin film electrode.[167, 168] Different from powder MMO with the tetragonal structure that is hard to intercalate $Mg^{2+}$, the cubic MMO thin film can be reversibly inserted/extracted with $Mg^{2+}$,[11, 169] which can be attributed to the improved ionic diffusion in the bulk and also at the SLI compared to MMO polymorph. Another consequence of the ionic diffusion at the interface is the result of the electrodeposition, or so-called dendrite formation at the metal anode. It has been shown that the dendrite can short the battery to cause safety issues. However, to increase the energy density (e.g., towards 500 kW/kg) of batteries the use of metals as the anode is necessary. The control of the dendrite formation at the metal anode and the inhibition of unwanted ionic diffusion at the SLI thus become challenging problems.[8] Numerous methods have been proposed to suppress, regulate and eliminate the dendrites in LEBs.[170-174] In particular, our group, in collaboration with Yang group at University of Central Florida, developed a ZnMn alloys (Figure 7a) that can achieve consistent superior performance under a high current density (80 $mA/cm^2$) over thousands of cycles (Figure 7b) in harsh electrochemical conditions, including testing in seawater-based aqueous electrolytes as the anode in multivalent aqueous batteries.[9] The alloy anode is synthesized by an electrodeposition method that involved the initiating growth on the electrode surface leading to clusters of alloy deposits which then combine to form a 3D structure. The *in-situ* optical visualization (Figure 7a) coupled with finite element analysis confirmed that the such structure at the SLI allows Zn to deposit easily inside the nano-voids, thus avoiding the dendrite formation. Those voids also allows other cations such as $Mg^{2+}$ and $Na^+$ in the seawater to adsorb.[9] Furthermore, the Zn ions would have a much faster deposition rate in the trench than that on the protruding region, which also minimized the dendrite formation (Figure 7).[9] With the help of XAS imaging (Figure 7c-7e), the reversible changes of anode in the charged and discharged states have been confirmed, suggesting the effectiveness of the strategy to inhibit the unwanted dendrite deposition at the SLI. This concept,

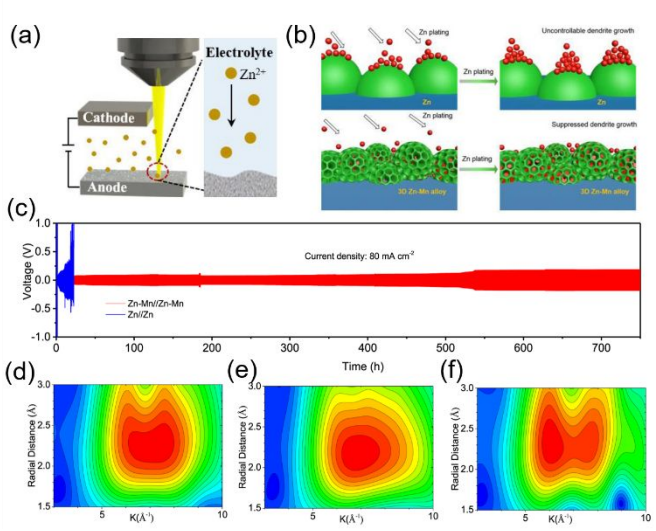


Figure 7: (a) schematic illustration of the in-situ optical visualization experimental setup (b) Schematic illustration of Zn plating processes on Zn anode (top) and Zn-Mn anode (bottom). (c) Long-term galvanostatic cycling performance of symmetric Zn-Mn and pristine Zn cells at a current density of 80 mA cm$^{-2}$ (areal capacity: 16 mAh cm$^{-2}$; Electrolyte: 2 M $ZnSO_4$ in seawater). Wavelet transform of Mn K-edge EXAFS for (d) pristine Zn-Mn anode, (e) fully discharged Zn-Mn anode, and (f) fully charged Zn-Mn anode.[9]

although demonstrated in aqueous battery, can result in a paradigm shift in the design of high-performance alloy anodes for both aqueous and non-aqueous batteries which will revolutionise the battery industries.

As seen in the discussions above, the interfacial processes at SLI are much more complicated than the SGI. However, no all of them lead to damage to the electrochemical energy devices. By understanding the formation and evolution of interfaces in reactions, one can come up with proper strategies to promote the positive and/or inhibit the negative interfacial processes with improved performance of the whole system.

## Liquid-gas Interface

Liquid-gas interface (LGI) is important but sometimes is ignored in many electrochemical energy devices involving gas reactants and liquid electrolytes, such as ORR and OER in metal-air batteries, ORR and hydrogen evolution reaction (HER) in fuel batteries, and CO2RR, and nitrogen reduction reaction (NRR).[175-178] For these systems, the dissolution and diffusion of gas reactants and subsequent reaction intermediates in liquid electrolytes can affect the overall reaction rates by changing the concentration of reactants transferring to the electrocatalysts and electrodes based on the chemical reaction rate law.[179, 180] For example, the higher concentration of alkaline electrolyte (e.g., 1 M of KOH) can provide more $OH^-$ ions that facilitate the transportation and formation of reaction intermediates (OH*) in ORR.[181-183] The mass transfer of gas reactants also depends on its diffusion rate and concentration that are related to the solubility of the gas. The quantitative study of the mass transfer in electrochemistry can be obtained using Levich Equation, where the Levich reaction current (or the limited current) depends on the diffusion coefficients, kinematic viscosity, angular rotation rate, and gas concentration. The dissolution directly affects the gas concentration.[184, 185] Some studies suggest using ionic electrolytes to improve the solubility of the gas in the electrolyte and then to increase the reaction rate.[138, 186-189] For example, Gittleson et al. systemically studied the oxygen transport in the electrolyte with both experimental and computational techniques.[189] Their results indicate that electrolyte salts would affect oxygen solubility (i.e. large anions such as TFSI- and BETI- increase oxygen solubility compared with smaller anions such as $BF_4^-$), and the solvents of electrolyte have an influence on the oxygen diffusivity. Besides the gas concentration, all the three left parameters (diffusion coefficients, kinematic viscosity, and angular rotation rate) influence the diffusion rate. For most inorganic electrolytes such as 1M KOH solutions, 1M $KHCO_3$ solutions, and 1M $H_2SO_4$ solutions used in energy devices mentioned above, the solubility of gases (e.g., $O_2$, $CO_2$, $H_2$) in those electrolytes is low, and the diffusion coefficient and the kinematic viscosity are constant. One way to improve the mass transfer is to increase the flow rate of the liquid containing the dissolved gas reactants to the electrodes. In rotating disk electrode experiments, this can be achieved by changing the electrode rotation speeds, and in practical fuel cell and metal-air devices, the flow electrolyte cell design can help.[190-193] Since the diffusion coefficient and kinematic viscosity are physical constants determining by the electrolyte itself, not many studies in electrocatalysis focus on those since the change of the electrolyte may also induce the change of electrolyte/electrode interfaces, thus making the system more complicated.

## Solid-Solid Interface

Solid-solid interface (SSI) is commonly found in many thin film devices such as semiconductor electronics. The epitaxial growth of oxides leads to heterostructured SSI that can be used as model systems to study electrochemical reactions such as batteries and catalysts.[92, 167, 168, 194-198] In SGI portion of this Feature Article, we have discussed a special solid-solid triple-phase boundary that involves ionic diffusion, charge transfer and restructuring at the electrolyte-cathode-gas interface. Here we will mainly focus on SSI in energy storage systems, particularly solid-state batteries (SSBs),[199-203] which use the non-flammable solid-state electrolytes (SSEs) instead of flammable liquid state electrolytes (LSEs). The advantages of using SSBs lie in not only their better safety than commercial LIBs, but also their compatibility with lithium metal anode to suppress the dendrite formation and gain high energy density.[10, 204-206] Hence, SSBs are one of the most promising next-generation energy storage systems to replace LIBs and have attracted significant amount of attentions from both academia and industries.[10, 204-206 207-210] Since repeated operations are needed to run SSBs, it requires high mechanical modulus and chemical stability for each component, particular the SSIs that connect two dissimilar materials. However, maintaining high stability at SSIs is challenging due to inevitable restructuring and possible side reactions at those interfaces. Some investigations have also found that SSBs are still suffered from the lithium dendrite formation, which causes electric short and then

shortens the batteries' cycle life.[211, 212] The improvement of interfacial properties at SSI becomes one of the most urgent tasks in battery community. Like the SEI in SLI in LIBs, the formation of an interphase layer at the solid electrode-electrolyte interface has recently been treated as a successful strategy to suppress dendrites' formation and maintain SSI stability. Zhang et al. reported that the *in-situ* formed nanoscale interface layer between novel poly(vinylidene difluoride) (PVDF)-based solid electrolytes and the Li anode leads to an open-circuiting feature instead of short-circuiting at high current density and avoids the risk of over-current, which can suppress Li dendrite growth.[213] Besides the *in-situ* self-formed SSI layer, Hou et al. demonstrated a LiF- and $Li_3N$-enriched artificial SSI constructed by *ex-situ* electroplating method[214] could stabilize metallic Li anode and improve the interface compatibility at the Li anode side to suppress the dendrite formation.[214]

Numerous studies have shown ways to modify and improve chemical and mechanical properties of SSI. However, relying on trial-and-error methods to design stable SSI is not trivial and rational. It is essential to first understand the interfacial processes at SSI including the formation of Li dendrite, the reactions and charge-transfer induced transformations. For example, to study the Li dendrite formation at the anode surface during cycling (Figure 8), Golozar et al. used the *in-situ* SEM combined with energy-dispersive spectroscopy (EDS),[20] and observed an apparent morphological change in the solid polymer electrolyte (SPE) when cycling the battery, which was believed to be the decomposition and degassing of the polymer electrolyte (Figure 8).[20] When increasing the cycling time, the dendrites were formed in the polymer regions causing further decomposition of the electrolyte at SSI, or some reaction between Li and the electrolyte (Figure 8).[20] They pointed out that the morphological change on the electrolyte caused by Li or decomposition interaction would be the problem for further Li dendrite growth and then the failure of the battery.[20] Moreover, Wang et al. applied time-resolved EIS and ultrasensitive 3D chemical analysis from time-of-flight secondary-ion mass spectrometry (ToF-SIMS) to study the intricated SSI and directly visualize the dendrite structures.[215] The results indicated that the electrolytes react with the metal electrodes at varying degrees upon contact, which contraries to the traditional options that dendrites were formed only in charging/discharging processes.[215] Those formed interphases widen the electrochemical window, but their electronic and ionic conductivities determine the battery performance and have a large influence on dendrite growth.[215] Based on the experiments results, they carried out the thermodynamic analysis on the interphase, and showed that an interphase with low electronic conductivity, high ionic conductivity, good chemical stability, a dynamic thickness and uniform coverage is good to prevent dendrite growth.[215] They also pointed out that the relatively stable electrolyte with the metal anode promotes fast dendrite growth, which does the general search for chemically stable electrolytes to improve the performance of SSBs helpless.[215]

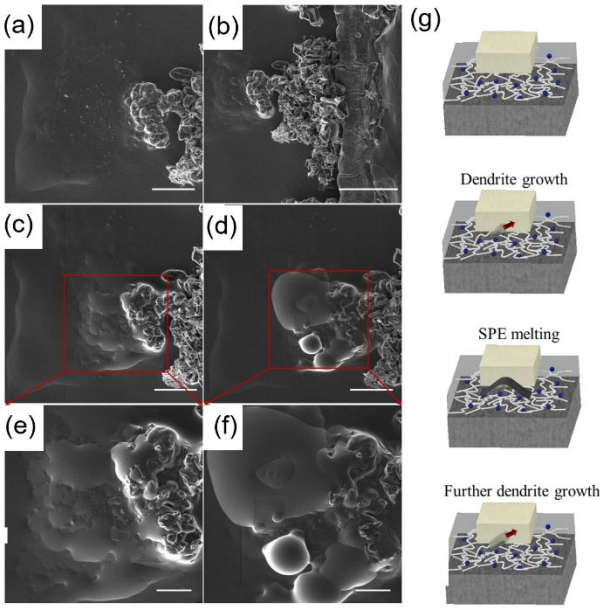


Figure 8: SEM images of the polymer and (g) schematic showing dendrite growth. SEM images. (a) After 3 days of cycling (scale bar representing 50 µm), (b) after 7 days of cycling (scale bar representing 100 µm), (c) after 9 days of cycling (scale bar representing 50 µm), and (d) after 13 days of cycling (scale bar representing 50 µm). (e) High magnification of the red box in image (c) (scale bar representing 20 µm), and (f) high magnification of the red box in image (d) showing the morphological change on the SPE (scale bar representing 20 µm). (g) Schematic of the dendrite formation and the effect of SPE melting on further dendrite growth.[20]

Figure 9: S 2p, Ge 3d, and P 2p XPS spectra and model fits for the pristine LGPS sample and after deposition of 31 nm Li metal. The identified species are marked and labeled in different colors. The small oxygen signal is caused by tiny fractions of oxygen in the atmosphere of the XPS chamber.[16]



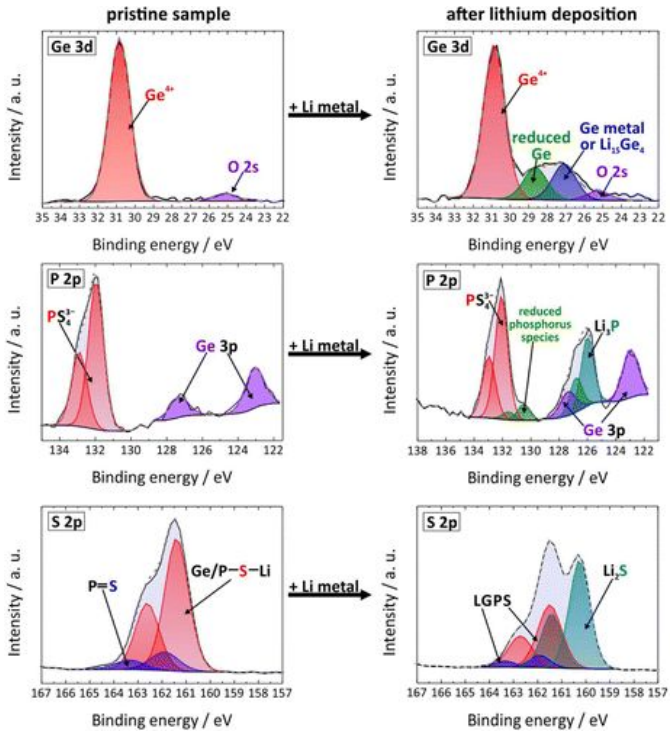


In addition to the dendrite formation in the anode-electrolyte interphase (AEI), the interfacial reactions between SSI and ions (e.g., $Li^+$) can form a passivation layer in the polymer-based electrolytes or an unstable interphase in sulfide-based electrolytes, thus affecting the SSBs performance. Since Lithium is a highly reductive metal, it can quickly extract hydrogen from the polymers or break the polymer backbone to form Li-O-R (R: organic groups such as $OCH_3$) types of compounds.[216, 217] Granvalet-Mancini et al. used atomic force microscopy (AFM) to show the formation of a passivation layer and attenuated total reflection Fourier transform infrared spectroscopy (FTIR) spectroscopy to detect the presence of $CF_3$ radicals in this passivation layer,[218] which has lower ionic conductivity and is bad for battery performance. One solution for preventing side reactions at SSI is to either in-situ form or ex-situ add an artificial stable layer on the AEI.[219-222] Li et al. grew a $Li_3PO_4$ thin film layer as an artificial AEI during the Li deposition/dissolution process.[221] The Li-conducting $Li_3PO_4$ layer can effectively reduce the side reactions between Li anode and polymer electrolyte.[221] Besides creating stable AEI, Zhang et al. developed a superior blends solid polymer electrolyte with integrated hierarchical architectures, which exhibits high ionic conductivity and good thermal stability.[220] Due to the unique structure and composition, a stable blend polymer and Li interphase were formed at the SSI, avoiding side reaction to form a passivation layer.[220] Similarly, sulfide-based electrolyte suffers from the similar situation as the polymer electrolytes. Once the Li anode encounters the sulfide-based electrolytes, the side reaction could happen to form the decomposition products such as $Li_2S$, unstable $Li_3P$, LiX (X= Cl, Br, I), and other compounds with remaining elements (Si, Ge, Sb,As, and Sn).[217, 223-226] Zhu et al. performed a first-principles study to estimate the decomposition energies of different solid electrolytes and suggested that $Li_{10}GeP_2S_{12}$ (LGPS) would decompose into $Li_3P_4$, $Li_2S$, and $Li_{15}Ge_4$, and $Li_3PS_4$ would decompose into $Li_3P$ and $Li_2S$.[199, 227] Later, Wenzel et al. utilized *in-situ* XPS to experimentally determine the compositions of the interphase during the electrochemical measurements.[16] They found that $Li_{10}GeP_2S_{12}$ decomposed to $Li_3P_4$, $Li_2S$, and some Li-Ge alloy (Figure 9), which is in perfect agreement with the theoretical predictions.[16] Clearly, the compositions of the anode-electrolyte interphase depend on the electrolytes (e.g., $Li_2S$ from $Li_3PS_4$[228]) and if the interphase is evitable, it should be formed with properties close to an ideal AEI with only Li-ion conductivity but no electron conductivity to block further reactions at the interface.[229, 230] An unstable AEI with both Li-ions and electrons conductivity will cause a continuous reaction between the lithium metal and the sulfide-based electrolyte, consuming both materials and reducing the cycle life of the SSBs.[229, 230] Like work done for the improvement of the stability at Li metal and polymer electrolyte interface, an artificial AEI layer that only conducts Li-ions with high compatibility to Li metal can be introduced to address the interfacial issues.[223, 231, 232] Simon et al. came up with a stable solid polymer electrolyte as a protection layer between Li anode and $Li_6PS_5Cl$ electrolyte. The XPS results confirmed that the polymer would form a durable interphase layer with $Li_6PS_5Cl$, consisting of polysulfides and LiF. The low resistance and easily formed layer protected $Li_6PS_5Cl$ from decomposition.[233] One has to be cautious that the interfacial reaction and dendrite growth can take place at the same time. Once the Li anode reacted with the electrolytes or grew into Li dendrite, it may recede a few microns, causing a worse connection between anode and electrolyte. Therefore, strong adhesion or surface modification between Li anode and electrolyte is a standard solution to ensure a good connection.[217]

Another SSI in SSBs is the cathode-electrolyte interface, which has less issues for Li dendrite formation. However, there are also ionic diffusion and charge transfer at such interface to form CEI. Like AEI, the cathode and electrolyte interfaces are mechanically rigid and can become unstable with an interphase layer during battery charging/discharging processes.[234-236] An interphase is predicted by the theoretical calculation and confirmed by XPS to form at the $LiCoO_2$/LiPON interface.[199, 237, 238] Later, Wang et al. conducted *in-situ* scanning transmission electron microscopy (STEM) coupled with electron energy loss spectroscopy (EELS) and revealed a disordered interfacial layer between $LiCoO_2$ and LiPON that accumulates Li and evolves to rocksalt CoO after cycling (Figure 10a-10f).[3] This CEI could be caused by the cathode reacting with the highly delithiated LiPON.[3] The increasing thickness of this layer would lead to rapid capacity decay as more of the cathode will be rendered electrochemically inactive.[3] Generally, CEI that allows both electron and ion transfers is very unstable and can cause continuous reactions of the electrolyte and the cathode.[199, 236] Zhang et al. also found that $LiCoO_2$/$Li_{10}GeP_2S_{12}$ interface was quite unstable and degraded in battery operation.[6] They used XRD to show the decrease of the grain size of the cycled $LiCoO_2$, which worsens the connection between the cathode and electrolyte (Figure 10g-10i).[6] Their EIS and XPS results suggested the decomposition products are a mixed electronic and ionic conductor, which allows for further oxidization of the electrolyte (Figure 9g-9i).[6] In some cases, CEI could conduct both Li and other ions, and subsequently leads to additional side reactions. Groh et al. demonstrated that Fe ions can diffuse through the $LiFeO_4$/$Li_{3+x}P_{1-x}Si_xO_4$ layer and react with $Li_{3+x}P_{1-x}Si_xO_4$ electrolyte,[239] which produces $LiFePO_4$–$Fe_2SiO_4$ and

$Li_3PO_4$–$Li_2FeSiO_4$, causing the capacity fading.[239] While in other cases, CEIs are just passivation layers with high resistance due to bad ionic and electronic conductivity.[234-236, 240, 241] As demonstrated by Kim et al. that $Li_7La_3Zr_2O_{12}$ would react with the $LiCoO_2$ to form an interphase layer (around 50nm thickness).[242] TOF-SIMS confirmed that the interphase consists of Al, Zr, La, and Co, affecting the initial Coulombic efficiency and cycle life.[242] To solve the instability of CEI or prevent side reactions at the interface, the similar strategy as used for AEI was applied by introducing an artificial SSI or protecting layer on the cathode.[217, 225, 243] For instances, the polyacrylonitrile (PAN)-based gel can soften and wet the cathode-electrolyte interface to reduce the whole battery's internal resistance.[244] $Li_2CoTi_3O_8$ was designed as an artificial SSI between $LiCoO_2$/$Li_{10}GeP_2S_{12}$ with high interfacial affinity due to thermodynamical and electrochemical compatibility with both cathode and electrolyte, thus enabling to excellent cyclability for the SSBs.[245]

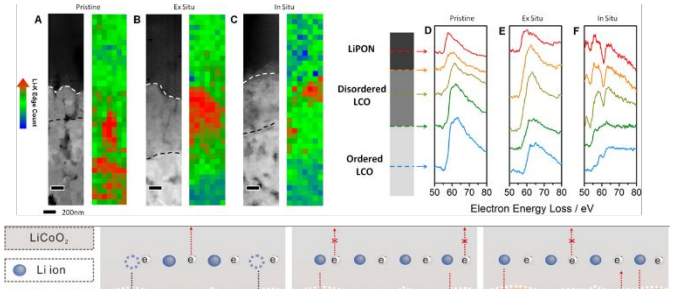


Figure 10: STEM image and EELS characterization. (a–c) High-angle annular dark-field image of the nanobattery stack along with Li K-edge concentration mapping of (a) pristine, (b) ex situ, and (c) in situ samples with scale bar represents 200 nm. (d–f) Li K-edge spectra from various parts of the layers are displayed for (d) pristine, (e) ex situ, and (f) in situ samples.[3] Schematic description of three possible situations occurring in a model SSBs with $LiCoO_2$ as the active material and LGPS as the solid electrode. (g) The ideal case: intimate contact between the SE and c-$LiCoO_2$, and no mutual reaction or decomposition of the SE. (h) Contact loss due to volume changes or failures during preparation. Decomposition of the SE at high voltages, forming a $Li^+$-depletion layer, thereby inhibiting Li+ mobility.[6]

As examples shown above, various interfacial processes take place at the SSI, which can lead to all kinds of interphases with different compositions and morphologies. It is essential to understand these processes, particularly during battery operation, and establish the structure-property relationship to guide battery design. Advanced characterizations are necessary for *in-situ* studies. Besides lab-based tools such as XPS, TEM, EELS, and ToF-SIMS, synchrotron X-ray scattering, spectroscopy and imaging techniques bring unique capabilities for studying the buried solid-solid interfaces to provide information related to materials' atomic as well as electronic structure, composition and morphology.[246, 247] Insights obtained from these studies can further help the development of stability SSIs for high performance SSBs.

## Summary and Perspective

The increasing demand of energy and high environmental standards on carbon neutral emission require the development of green, sustainable energy storage and conversion devices. Electrochemical energy systems, due to their zero or negative carbon emission, have raised as the promising candidates. However, to enable large-scale applications, their performances must be further improved, which lies in the reduction of unwanted side reactions and products to achieve high efficiency and good stability. A lot of issues have been identified at interfaces which are key components in these systems as they connect electrodes and electrolyte together. Improvement in electrode-electrolyte interfaces can lead to the advancement of the whole systems. Therefore, we review and discuss various interfacial processes, including electron/charge transfer, ionic transfer, surface reconstruction and adsorption/desorption, in three interfaces, namely solid-gas, solid-liquid and solid-solid. Owning to their unique combinations, representative electrochemical energy systems are chosen and illustrated accordingly. The three interfaces change differently and can have either positive or negative effects on the performance of the electrochemical energy devices. Hence, we should deal with the interfaces case by case. For solid-gas interfaces, the gas adsorption is the first step of all interfacial processes. The construction of beneficial interfaces (e.g., DPB and TPB) mush have an effective function to facilitate the adsorption, diffusion, and reaction of gas molecules. Considering the ionic and electron transfer associated with the reactions at the solid-gas interfaces, the electrodes are preferred to be the mixed ionic and electronic conductors while the electrolyte is only allowed to conduct ions. The DPB and TBP should be able to tolerate the structural and composition changes induced by gas/ion diffusion and interaction. For solid-liquid interfaces, charge-transfer and ion-transfer are two major processes that can result in various unwanted or desired interfacial changes such as adsorption/desorption of reaction intermediates, surface restructuring and deposition. In electrocatalysis, charge-transfer is related to the electronic structure at interfaces. Tuning the proper electronic structure (e.g., metal *d*-band center and oxygen *p*-band center) can achieve optimal adsorptive power for reaction molecules or intermediates with less undesired surface restructuring. In liquid-electrolyte-based batteries, ion-transfer is the dominant process that can lead to interfacial restructuring and the formation of interphases, which sometimes are facilitated by charge-transfer process and are quite complicated. Although SEI is known to be beneficial for lithium-ion batteries, it is not always a good interphase in other batteries such as multivalent batteries. If the interfacial restructuring is inevitable, one should make sure that the formation of interphase(s) can only permit ion-transfer instead of electron-transfer at the solid-liquid interfaces in batteries and maintain the structural stability during ionic diffusion through the electrodes. For solid-solid interfaces, the major effort right now is to reduce the interfacial resistances and metal dendrite formation in solid-state batteries. Promising results have been achieved by modifying and improving chemical and mechanical properties of solid-solid interfaces so that the ion-transfer and electron transfer can result in less undesired interfacial restructuring. Of these interfaces, we only review limited examples, and in most cases, these interfacial processes are coupled together, and complicated changes are induced at electrode-electrolyte interfaces. Besides reviewing what occur at these interfaces, we also discuss strategies to modify interfaces for desired properties. In addition, we emphasize the importance of *in-situ* and *operando* characterizations, particularly synchrotron X-ray techniques, in understanding these interfacial processes during the operation of the electrochemical energy systems. The goal of future studies of

complex interfacial processes is to establish clear structure-property relationship that can link changes at electrode-electrolyte interfaces to the overall performance at the device level, thus providing guidance to advance the technology of electrochemical energy storage and conversion systems to meet the society development.

## Conflicts of interest

There are no conflicts to declare.

## Acknowledgements

This work was supported by the National Science Foundation under Grant No. CBET-1949870, CBET-2016192, and DMR-1832803.

## Table of contents

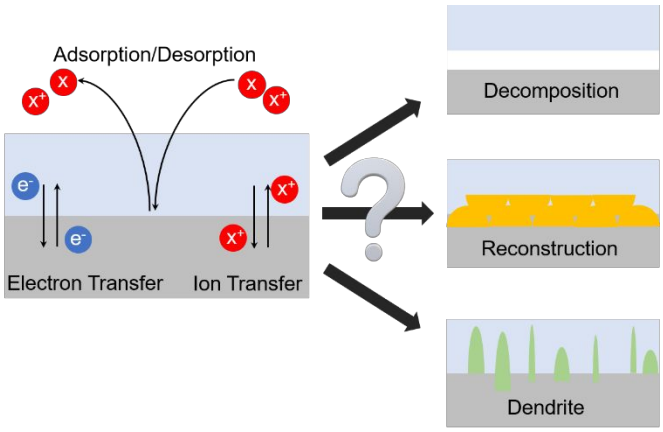


## References

1. C. R. Kreller, T. J. McDonald, S. B. Adler, E. J. Crumlin, E. Mutoro, S. J. Ahn, G. J. la O', Y. Shao-Horn, M. D. Biegalski, H. M. Christen, R. R. Chater and J. A. Kilner, *J Electrochem Soc*, 2013, **160**, F931-F942.
2. C. Cai, M. Y. Wang, S. B. Han, Q. Wang, Q. Zhang, Y. M. Zhu, X. M. Yang, D. J. Wu, X. T. Zu, G. E. Sterbinsky, Z. X. Feng and M. Gu, *ACS Catalysis*, 2021, **11**, 123-130.
3. Z. Y. Wang, D. Santhanagopalan, W. Zhang, F. Wang, H. L. L. Xin, K. He, J. C. Li, N. Dudney and Y. S. Meng, *Nano Lett*, 2016, **16**, 3760-3767.
4. Z. X. Feng, Y. Yacoby, M. J. Gadre, Y. L. Lee, W. T. Hong, H. Zhou, M. D. Biegalski, H. M. Christen, S. B. Adler, D. Morgan and Y. Shao-Horn, *J Phys Chem Lett*, 2014, **5**, 1027-1034.
5. Z. X. Feng, E. J. Crumlin, W. T. Hong, D. Lee, E. Mutoro, M. D. Biegalski, H. Zhou, H. Bluhm, H. M. Christen and Y. Shao-Horn, *J Phys Chem Lett*, 2013, **4**, 1512-1518.
6. W. B. Zhang, F. H. Richter, S. P. Culver, T. Leichtweiss, J. G. Lozano, C. Dietrich, P. G. Bruce, W. G. Zeier and J. Janek, *ACS Applied Materials & Interfaces*, 2018, **10**, 22226-22236.
7. R. R. Rao, M. J. Kolb, N. B. Halck, A. F. Pedersen, A. Mehta, H. You, K. A. Stoerzinger, Z. X. Feng, H. A. Hansen, H. Zhou, L. Giordano, J. Rossmeisl, T. Vegge, I. Chorkendorff, I. E. L. Stephens and Y. Shao-Horn, *Energ Environ Sci*, 2017, **10**, 2626-2637.
8. J. Xiao, *Science*, 2019, **366**, 426-427.
9. H. Tian, Z. Li, G. Feng, Z. Yang, D. Fox, M. Wang, H. Zhou, L. Zhai, A. Kushima, Y. Du, Z. Feng, X. Shan and Y. Yang, *Nature Communications*, 2021, **12**, 237.
10. J. Yue, X. Y. Zhu, F. D. Han, X. L. Fan, L. N. Wang, J. Yang and C. S. Wang, *ACS Applied Materials & Interfaces*, 2018, **10**, 39645-39650.
11. M. Y. Wang, B. H. Han, J. J. Deng, Y. Jiang, M. Y. Zhou, M. Lucero, Y. Wang, Y. B. Chen, Z. Z. Yang, A. T. N'Diaye, Q. Wang, Z. C. J. Xu and Z. X. Feng, *ACS Applied Materials & Interfaces*, 2019, **11**, 5682-5686.
12. Z. Weng, J. B. Jing, Y. S. Wu, Z. S. Wu, X. T. Guo, K. L. Materna, W. Liu, V. S. Batista, G. W. Brudvig and H. L. Wang, *J Am Chem Soc*, 2016, **138**, 8076-8079.
13. S. Qiu, X. Y. Wu, M. Y. Wang, M. Lucero, Y. Wang, J. Wang, Z. Z. Yang, W. Q. Xu, Q. Wang, M. Gu, J. G. Wen, Y. Q. Huang, Z. C. J. Xu and Z. X. Feng, *Nano Energy*, 2019, **64**, 103941.
14. G. M. Rupp, A. K. Opitz, A. Nenning, A. Limbeck and J. Fleig, *Nature Materials*, 2017, **16**, 640-650.
15. P. X. Bai, Y. W. He, P. X. Xiong, X. X. Zhao, K. Xu and Y. H. Xu, *Energy Storage Mater*, 2018, **13**, 274-282.
16. S. Wenzel, S. Randau, T. Leichtweiss, D. A. Weber, J. Sann, W. G. Zeier and J. Janek, *Chemistry of Materials*, 2016, **28**, 2400-2407.
17. D. D. Wang, Q. Z. Yan, M. Q. Li, H. P. Gao, J. H. Tian, Z. Q. Shan, N. Wang, J. Luo, M. Zhou and Z. Chen, *Nanoscale*, 2021, **13**, 2811-2819.
18. A. Friesen, S. Hildebrand, F. Horsthemke, M. Borner, R. Klopsch, P. Niehoff, F. M. Schappacher and M. Winter, *J Power Sources*, 2017, **363**, 70-77.
19. J. Y. Wang, W. Huang, A. Pei, Y. Z. Li, F. F. Shi, X. Y. Yu and Y. Cui, *Nat Energy*, 2019, **4**, 664-670.
20. M. Golozar, A. Paolella, H. Demers, S. Bessette, M. Lagace, P. Bouchard, A. Guerfi, R. Gauvin and K. Zaghib, *Commun Chem*, 2019, **2**, 131.
21. S. Y. Luchkin, S. A. Lipovskikh, N. S. Katorova, A. A. Savina, A. M. Abakumov and K. J. Stevenson, *Sci Rep-Uk*, 2020, **10**, 8550.
22. L. M. Suo, D. Oh, Y. X. Lin, Z. Q. Zhuo, O. Borodin, T. Gao, F. Wang, A. Kushima, Z. Q. Wang, H. C. Kim, Y. Qi, W. L. Yang, F. Pan, J. Li, K. Xu and C. S. Wang, *J Am Chem Soc*, 2017, **139**, 18670-18680.
23. K. Macounova, M. Makarova, J. Franc, J. Jirkovsky and P. Krtil, *Electrochem Solid St*, 2008, **11**, F27-F29.
24. Y. Duan, S. N. Sun, S. B. Xi, X. Ren, Y. Zhou, G. L. Zhang, H. T. Yang, Y. H. Du and Z. C. J. Xu, *Chemistry of Materials*, 2017, **29**, 10534-10541.
25. M. Wang, B. Han, J. Deng, Y. Jiang, M. Zhou, M. Lucero, Y. Wang, Y. Chen, Z. Yang, A. T. N'Diaye, Q. Wang, Z. J. Xu and

Z. Feng, *ACS Applied Materials & Interfaces*, 2019, **11**, 5682-5686.
26. Z. L. Wang, D. Xu, J. J. Xu and X. B. Zhang, *Chem Soc Rev*, 2014, **43**, 7746-7786.
27. Y. Y. Zhang, H. W. Lei, D. L. Duan, E. Villota, C. Liu and R. Ruan, *ACS Applied Materials & Interfaces*, 2018, **10**, 20429-20439.
28. P. Y. Wang, M. Y. Yan, J. S. Meng, G. P. Jiang, L. B. Qu, X. L. Pan, J. Z. Liu and L. Q. Mai, *Nature Communications*, 2017, **8**, 645.
29. J. Tymoczko, F. Calle-Vallejo, V. Colic, M. T. M. Koper, W. Schuhmann and A. S. Bandarenka, *ACS Catalysis*, 2014, **4**, 3772-3778.
30. W. T. Hong, K. A. Stoerzinger, Y. L. Lee, L. Giordano, A. Grimaud, A. M. Johnson, J. Hwang, E. J. Crumlin, W. L. Yang and Y. Shao-Horn, *Energ Environ Sci*, 2017, **10**, 2190-2200.
31. F. Wang, O. Borodin, M. S. Ding, M. Gobet, J. Vatamanu, X. L. Fan, T. Gao, N. Eidson, Y. J. Liang, W. Sun, S. Greenbaum, K. Xu and C. S. Wang, *Joule*, 2018, **2**, 2178-2178.
32. J. Asenbauer, T. Eisenmann, M. Kuenzel, A. Kazzazi, Z. Chen and D. Bresser, *Sustain Energ Fuels*, 2020, **4**, 5387-5416.
33. M. Agostini, B. Scrosati and J. Hassoun, *Adv Energy Mater*, 2015, **5**, 1500481.
34. L. M. Suo, O. Borodin, T. Gao, M. Olguin, J. Ho, X. L. Fan, C. Luo, C. S. Wang and K. Xu, *Science*, 2015, **350**, 938-943.
35. X. Q. Zhang, M. F. Dong, Y. L. Xiong, Z. G. Hou, H. S. Ao, M. K. Liu, Y. C. Zhu and Y. T. Qian, *Small*, 2020, **16**, 2003585.
36. X. T. Xi, W. H. Li, B. H. Hou, Y. Yang, Z. Y. Gu and X. L. Wu, *ACS Appl Energ Mater*, 2019, **2**, 201-206.
37. K. A. Stoerzinger, M. Favaro, P. N. Ross, Z. Hussain, Z. Liu, J. Yano and E. J. Crumlin, *Top Catal*, 2018, **61**, 2152-2160.
38. A. J. Tkalych, H. L. L. Zhuang and E. A. Carter, *ACS Catalysis*, 2017, **7**, 5329-5339.
39. H. Ali-Loytty, M. W. Louie, M. R. Singh, L. Li, H. G. S. Casalongue, H. Ogasawara, E. J. Crumlin, Z. Liu, A. T. Bell, A. Nilsson and D. Friebel, *J Phys Chem C*, 2016, **120**, 2247-2253.
40. B. R. Wygant, K. Kawashima and C. B. Mullins, *ACS Energy Letters*, 2018, **3**, 2956-2966.
41. S. T. Christensen, B. Lee, Z. X. Feng, M. C. Hersam and M. J. Bedzyk, *Appl Surf Sci*, 2009, **256**, 423-427.
42. S. T. Christensen, J. W. Elam, B. Lee, Z. Feng, M. J. Bedzyk and M. C. Hersam, *Chemistry of Materials*, 2009, **21**, 516-521.
43. Z. Li, S. F. Ji, Y. W. Liu, X. Cao, S. B. Tian, Y. J. Chen, Z. G. Niu and Y. D. Li, *Chem Rev*, 2020, **120**, 623-682.
44. G. A. Somorjai and Y. Li, *Introduction to surface chemistry and catalysis*, Wiley, Hoboken, N.J., 2nd edn., 2010.
45. J. M. Dreimann, E. Kohls, H. F. W. Warmeling, M. Stein, L. F. Guo, M. Garland, T. N. Dinh and A. J. Vorholt, *ACS Catalysis*, 2019, **9**, 4308-4319.
46. C. Barroo, Z. J. Wang, R. Schloegl and M. G. Willinger, *Nat Catal*, 2020, **3**, 30-39.
47. Z. Feng, Q. Ma, J. Lu, H. Feng, J. W. Elam, P. C. Stair and M. J. Bedzyk, *Rsc Adv*, 2015, **5**, 103834-103840.
48. H. J. Freund and G. Pacchioni, *Chem Soc Rev*, 2008, **37**, 2224-2242.
49. H. J. Freund, *Surf Sci*, 2002, **500**, 271-299.
50. M. Baumer and H. J. Freund, *Prog Surf Sci*, 1999, **61**, 127-198.
51. B. J. Xu, X. Y. Liu, J. Haubrich and C. M. Friend, *Nat Chem*, 2010, **2**, 61-65.
52. B. C. Wiegand and C. M. Friend, *Chem Rev*, 1992, **92**, 491-504.
53. B. K. Min and C. M. Friend, *Chem Rev*, 2007, **107**, 2709-2724.
54. Z. Feng, M. E. McBriarty, A. U. Mane, J. Lu, P. C. Stair, J. W. Elam and M. J. Bedzyk, *Rsc Adv*, 2014, **4**, 64608-64616.
55. Z. X. Feng, J. L. Lu, H. Feng, P. C. Stair, J. W. Elam and M. J. Bedzyk, *J Phys Chem Lett*, 2013, **4**, 285-291.
56. Z. X. Feng, L. Cheng, C. Y. Kim, J. W. Elam, Z. Zhang, L. A. Curtiss, P. Zapol and M. J. Bedzyk, *J Phys Chem Lett*, 2012, **3**, 2845-2850.
57. Z. X. Feng, S. T. Christensen, J. W. Elam, B. Lee, M. C. Hersam and M. J. Bedzyk, *J Appl Phys*, 2011, **110**, 102202.
58. Z. X. Feng, A. Kazimirov and M. J. Bedzyk, *Acs Nano*, 2011, **5**, 9755-9760.
59. Z. X. Feng, C. Y. Kim, J. W. Elam, Q. Ma, Z. Zhang and M. J. Bedzyk, *J Am Chem Soc*, 2009, **131**, 18200.
60. A. Berenov, A. Atkinson, J. Kilner, M. Ananyev, V. Eremin, N. Porotnikova, A. Farlenkov, E. Kurumchin, H. J. M. Bouwmeester, E. Bucher and W. Sitte, *Solid State Ionics*, 2014, **268**, 102-109.
61. W. Lee, H. J. Jung, M. H. Lee, Y. B. Kim, J. S. Park, R. Sinclair and F. B. Prinz, *Adv Funct Mater*, 2012, **22**, 965-971.
62. S. Hong, H. Yang, Y. Lim, F. B. Prinz and Y. B. Kim, *ACS Applied Materials & Interfaces*, 2019, **11**, 41338-41346.
63. M. Kubicek, Z. H. Cai, W. Ma, B. Yildiz, H. Hutter and J. Fleig, *Acs Nano*, 2013, **7**, 3276-3286.
64. F. F. Dong, Y. B. Chen, D. J. Chen and Z. P. Shao, *ACS Applied Materials & Interfaces*, 2014, **6**, 11180-11189.
65. S. B. Adler, J. A. Lane and B. C. H. Steele, *J Electrochem Soc*, 1996, **143**, 3554-3564.
66. S. B. Adler, *Solid State Ionics*, 1998, **111**, 125-134.
67. W. C. Chueh and S. M. Haile, *Annu Rev Chem Biomol*, 2012, **3**, 313-341.
68. S. L. Pang, G. M. Yang, X. N. Jiang, X. Q. Shen, D. W. Rao and C. L. Chen, *J Catal*, 2020, **381**, 408-414.
69. G. M. Yang, W. Zhou, M. L. Liu and Z. P. Shao, *ACS Applied Materials & Interfaces*, 2016, **8**, 35308-35314.
70. E. Mutoro, E. J. Crumlin, M. D. Biegalski, H. M. Christen and Y. Shao-Horn, *Energ Environ Sci*, 2011, **4**, 3689-3696.
71. Z. L. Jian, W. T. Wang, M. Y. Wang, Y. Wang, N. AuYeung, M. Liu and Z. X. Feng, *Chinese Chem Lett*, 2018, **29**, 1768-1772.
72. G. J. la O', S. J. Ahn, E. Crumlin, Y. Orikasa, M. D. Biegalski, H. M. Christen and Y. Shao-Horn, *Angew Chem Int Edit*, 2010, **49**, 5344-5347.
73. E. J. Crumlin, E. Mutoro, Z. Liu, M. E. Grass, M. D. Biegalski, Y. L. Lee, D. Morgan, H. M. Christen, H. Bluhm and Y. Shao-Horn, *Energ Environ Sci*, 2012, **5**, 6081-6088.
74. T. C. Geary, D. Lee, Y. Shao-Horn and S. B. Adler, *J Electrochem Soc*, 2016, **163**, F1107-F1114.
75. E. Mutoro, E. J. Crumlin, H. Popke, B. Luerssen, M. Amati, M. K. Abyaneh, M. D. Biegalski, H. M. Christen, L. Gregoratti, J. Janek and Y. Shao-Horn, *J Phys Chem Lett*, 2012, **3**, 40-44.
76. M. Li, M. H. Zheng, B. B. Hu, Y. X. Zhang and C. R. Xia, *Electrochim Acta*, 2017, **230**, 196-203.
77. X. Xu, C. Wang, M. Fronzi, X. Liu, L. Bi and X. S. Zhao, *Materials for Renewable and Sustainable Energy*, 2019, **8**, 15.
78. Y. Chen, A. Hinerman, L. Liang, K. Gerdes, S. P. Navia, J. Prucz and X. Y. Song, *J Power Sources*, 2018, **405**, 45-50.

79. J. D. Fehribach and R. O'Hayre, *Siam J Appl Math*, 2009, **70**, 510-530.
80. Y. Yan, S. C. Sandu, J. Conde and P. Muralt, *J Power Sources*, 2012, **206**, 84-90.
81. M. H. Wu, J. L. Huang, K. Z. Fung and D. F. Lii, *Surf Coat Tech*, 2010, **205**, 30-34.
82. T. M. M. Heenan, J. J. Bailey, X. Lu, J. B. Robinson, F. Iacoviello, D. P. Finegan, D. J. L. Brett and P. R. Shearing, *Fuel Cells*, 2017, **17**, 75-82.
83. S. Ricciardi, J. C. Ruiz-Morales and P. Nunez, *Solid State Ionics*, 2009, **180**, 1083-1090.
84. S. Zhang and A. M. Gokhale, *J Power Sources*, 2012, **219**, 172-179.
85. G. F. Cai, Y. L. Zhang, H. L. Dai, S. C. He, L. Ge, H. Chen and L. C. Guo, *Mater Lett*, 2017, **195**, 232-235.
86. W. Jeong, W. Yu, M. S. Lee, S. J. Bai, G. Y. Cho and S. W. Cha, *Int J Hydrogen Energ*, 2020, **45**, 32442-32448.
87. N. Vivet, S. Chupin, E. Estrade, A. Richard, S. Bonnamy, D. Rochais and E. Bruneton, *J Power Sources*, 2011, **196**, 9989-9997.
88. Y. Chen, Z. H. Cai, Y. Kuru, W. Ma, H. L. Tuller and B. Yildiz, *Adv Energy Mater*, 2013, **3**, 1221-1229.
89. Z. X. Feng, Y. Yacoby, W. T. Hong, H. Zhou, M. D. Biegalski, H. M. Christen and Y. Shao-Horn, *Energ Environ Sci*, 2014, **7**, 1166-1174.
90. Y.-L. Lee, J. Kleis, J. Rossmeisl, Y. Shao-Horn and D. Morgan, *Energ Environ Sci*, 2011, **4**, 3966-3970.
91. Y. L. Lee, J. Kleis, J. Rossmeisl and D. Morgan, *Phys Rev B*, 2009, **80**, 224101.
92. J. Hwang, Z. X. Feng, N. Charles, X. R. Wang, D. Lee, K. A. Stoerzinger, S. Muy, R. R. Rao, D. Lee, R. Jacobs, D. Morgan and Y. Shao-Horn, *Mater Today*, 2019, **31**, 100-118.
93. J. Hwang, K. Akkiraju, J. Corchado-Garcia and Y. Shao-Horn, *J Phys Chem C*, 2019, **123**, 24469-24476.
94. Y. Chen, D. D. Fong, F. W. Herbert, J. Rault, J. P. Rueff, N. Tsvetkov and B. Yildiz, *Chemistry of Materials*, 2018, **30**, 3359-3371.
95. X. F. Yang, J. Hu, J. Fu, R. Q. Wu and B. E. Koel, *Angew Chem Int Edit*, 2011, **50**, 10182-10185.
96. H. Y. Zhu, S. Zhang, D. Su, G. M. Jiang and S. H. Sun, *Small*, 2015, **11**, 3545-3549.
97. Y. Jiao, Y. Zheng, M. T. Jaroniec and S. Z. Qiao, *Chem Soc Rev*, 2015, **44**, 2060-2086.
98. S. Ko, Y. Yamada and A. Yamada, *ACS Applied Materials & Interfaces*, 2019, **11**, 45554-45560.
99. H. T. Zhang, D. Y. Wang and C. Shen, *Appl Surf Sci*, 2020, **507**, 145059.
100. B. Hammer and J. K. Norskov, *Adv Catal*, 2000, **45**, 71-129.
101. J. K. Norskov, J. Rossmeisl, A. Logadottir, L. Lindqvist, J. R. Kitchin, T. Bligaard and H. Jonsson, *J Phys Chem B*, 2004, **108**, 17886-17892.
102. Z. Y. Duan and G. F. Wang, *J Phys Chem C*, 2013, **117**, 6284-6292.
103. J. Greeley, I. E. L. Stephens, A. S. Bondarenko, T. P. Johansson, H. A. Hansen, T. F. Jaramillo, J. Rossmeisl, I. Chorkendorff and J. K. Norskov, *Nat Chem*, 2009, **1**, 552-556.
104. C. Chen, Y. J. Kang, Z. Y. Huo, Z. W. Zhu, W. Y. Huang, H. L. L. Xin, J. D. Snyder, D. G. Li, J. A. Herron, M. Mavrikakis, M. F. Chi, K. L. More, Y. D. Li, N. M. Markovic, G. A. Somorjai, P. D. Yang and V. R. Stamenkovic, *Science*, 2014, **343**, 1339-1343.
105. R. R. Rao, M. J. Kolb, J. Hwang, A. F. Pedersen, A. Mehta, H. You, K. A. Stoerzinger, Z. X. Feng, H. Zhou, H. Bluhm, L. Giordano, I. E. L. Stephens and Y. Shao-Horn, *J Phys Chem C*, 2018, **122**, 17802-17811.
106. N. Alonso-Vante, P. Borthen, M. Fieber-Erdmann, H. H. Strehblow and E. Holub-Krappe, *Electrochim Acta*, 2000, **45**, 4227-4236.
107. D. Y. Kuo, J. K. Kawasaki, J. N. Nelson, J. Kloppenburg, G. Hautier, K. M. Shen, D. G. Schlom and J. Suntivich, *J Am Chem Soc*, 2017, **139**, 3473-3479.
108. J. J. Velasco-Velez, V. Pfeifer, M. Havecker, R. S. Weatherup, R. Arrigo, C. H. Chuang, E. Stotz, G. Weinberg, M. Salmeron, R. Schlogl and A. Knop-Gericke, *Angew Chem Int Edit*, 2015, **54**, 14554-14558.
109. H. F. Feng, X. Xu, Y. Du and S. X. Dou, *Electrochem Energy R*, 2021, 249–268.
110. J. H. Bang and H. Kim, *B Korean Chem Soc*, 2011, **32**, 3660-3665.
111. L. Wang, Q. Zhou, Z. H. Pu, Q. Zhang, X. Q. Mu, H. Y. Jing, S. L. Liu, C. Y. Chen and S. C. Mu, *Nano Energy*, 2018, **53**, 270-276.
112. W. Z. Tu, K. Chen, L. J. Zhu, H. C. Zai, E. Bin, X. X. Ke, C. F. Chen, M. L. Sui, Q. Chen and Y. J. Li, *Adv Funct Mater*, 2019, **29**, 1807070.
113. Y. Y. Li, X. C. Du, J. W. Huang, C. Y. Wu, Y. H. Sun, G. F. Zou, C. T. Yang and J. Xiong, *Small*, 2019, **15**, 1901980.
114. Y. F. Wang, D. Sun, M. Y. Wang, Z. X. Feng and A. S. Hall, *J Phys Chem C*, 2020, **124**, 5220-5224.
115. Q. F. Gong, P. Ding, M. Q. Xu, X. R. Zhu, M. Y. Wang, J. Deng, Q. Ma, N. Han, Y. Zhu, J. Lu, Z. X. Feng, Y. F. Li, W. Zhou and Y. G. Li, *Nature Communications*, 2019, **10**, 2807.
116. X. Zhang, Y. Wang, M. Gu, M. Y. Wang, Z. S. Zhang, W. Y. Pan, Z. Jiang, H. Z. Zheng, M. Lucero, H. L. Wang, G. E. Sterbinsky, Q. Ma, Y. G. Wang, Z. X. Feng, J. Li, H. J. Dai and Y. Y. Liang, *Nat Energy*, 2020, **5**, 684-692.
117. Y. S. Wu, J. B. Jiang, Z. Weng, M. Y. Wang, D. L. J. Broere, Y. R. Zhong, G. W. Brudvig, Z. X. Feng and H. L. Wang, *ACS Central Science*, 2017, **3**, 847-852.
118. G. Y. Chen, K. A. Kuttiyiel, M. Li, D. Su, L. Du, C. Y. Du, Y. Z. Gao, W. D. Fei, G. P. Yin, K. Sasaki and R. R. Adzic, *Journal of Materials Chemistry A*, 2018, **6**, 20725-20736.
119. R. Majee, Q. A. Islam, S. Mondal and S. Bhattacharyya, *Chem Sci*, 2020, **11**, 10180-10189.
120. C. W. Tung, Y. Y. Hsu, Y. P. Shen, Y. X. Zheng, T. S. Chan, H. S. Sheu, Y. C. Cheng and H. M. Chen, *Nature Communications*, 2015, **6**, 8106.
121. C. Wei, Z. X. Feng, G. G. Scherer, J. Barber, Y. Shao-Horn and Z. C. J. Xu, *Advanced Materials*, 2017, **29**, 1606800.
122. C. Wei, Z. X. Feng, M. Baisariyev, L. H. Yu, L. Zeng, T. P. Wu, H. Y. Zhao, Y. Q. Huang, M. J. Bedzyk, T. Sritharan and Z. C. J. Xu, *Chemistry of Materials*, 2016, **28**, 4129-4133.
123. Z. Weng, Y. S. Wu, M. Y. Wang, J. B. Jiang, K. Yang, S. J. Huo, X. F. Wang, Q. Ma, G. W. Brudvig, V. S. Batista, Y. Y. Liang, Z. X. Feng and H. L. Wang, *Nature Communications*, 2018, **9**, 415.
124. J. Suntivich, K. J. May, H. A. Gasteiger, J. B. Goodenough and Y. Shao-Horn, *Science*, 2011, **334**, 1383-1385.
125. K. J. May, C. E. Carlton, K. A. Stoerzinger, M. Risch, J. Suntivich, Y. L. Lee, A. Grimaud and Y. Shao-Horn, *J Phys Chem Lett*, 2012, **3**, 3264-3270.
126. L. C. Seitz, C. F. Dickens, K. Nishio, Y. Hikita, J. Montoya, A.

Doyle, C. Kirk, A. Vojvodic, H. Y. Hwang, J. K. Norskov and T. F. Jaramillo, *Science*, 2016, **353**, 1011-1014.
127. G. Wan, J. W. Freeland, J. Kloppenburg, G. Petretto, J. N. Nelson, D. Y. Kuo, C. J. Sun, J. G. Wen, J. T. Diulus, G. S. Herman, Y. Q. Dong, R. H. Kou, J. Y. Sun, S. Chen, K. M. Shen, D. G. Schlom, G. M. Rignanese, G. Hautier, D. D. Fong, Z. X. Feng, H. Zhou and J. Suntivich, *Science Advances*, 2021, **7**, eabc7323.
128. P. S. Li, M. Y. Wang, X. X. Duan, L. R. Zheng, X. P. Cheng, Y. F. Zhang, Y. Kuang, Y. P. Li, Q. Ma, Z. X. Feng, W. Liu and X. M. Sun, *Nature Communications*, 2019, **10**, 1711.
129. Z. Cai, D. J. Zhou, M. Y. Wang, S. M. Bak, Y. S. Wu, Z. S. Wu, Y. Tian, X. Y. Xiong, Y. P. Li, W. Liu, S. Siahrostami, Y. Kuang, X. Q. Yang, H. H. Duan, Z. X. Feng, H. L. Wang and X. M. Sun, *Angew Chem Int Edit*, 2018, **57**, 9392-9396.
130. C. Hu, E. H. Song, M. Y. Wang, W. Chen, F. Q. Huang, Z. X. Feng, J. J. Liu and J. C. Wang, *Adv Sci*, 2021, **8**, 2001881.
131. M. Y. Wang, L. Arnadottir, Z. C. J. Xu and Z. X. Feng, *Nano-Micro Lett*, 2019, **11**.
132. Y. Zhao, X. Tan, W. F. Yang, C. Jia, X. J. Chen, W. H. Ren, S. C. Smith and C. Zhao, *Angew Chem Int Edit*, 2020, **59**, 21493-21498.
133. S. H. Lee, J. C. Lin, M. Farmand, A. T. Landers, J. T. Feaster, J. E. A. Acosta, J. W. Beeman, Y. F. Ye, J. Yano, A. Mehta, R. C. Davis, T. F. Jaramillo, C. Hahn and W. S. Drisdell, *J Am Chem Soc*, 2021, **143**, 588-592.
134. S. Verma, X. Lu, S. C. Ma, R. I. Masel and P. J. A. Kenis, *Phys Chem Chem Phys*, 2016, **18**, 7075-7084.
135. Y. P. Wijaya, K. J. Smith, C. S. Kim and E. L. Gyenge, *J Appl Electrochem*, 2021, **51**, 51-63.
136. G. F. Li, M. Divinagracia, M. F. Labata, J. D. Ocon and P. Y. A. Chuang, *ACS Applied Materials & Interfaces*, 2019, **11**, 33748-33758.
137. J. A. Arminio-Ravelo, A. W. Jensen, K. D. Jensen, J. Quinson and M. Escudero-Escribano, *Chemphyschem*, 2019, **20**, 2956-2963.
138. A. C. Garcia and M. T. M. Koper, *Acs Catalysis*, 2018, **8**, 9359-9363.
139. V. Colic, M. D. Pohl, D. Scieszka and A. S. Bandarenka, *Catal Today*, 2016, **262**, 24-35.
140. M. M. Waegele, C. M. Gunathunge, J. Y. Li and X. Li, *J Chem Phys*, 2019, **151**, 160902.
141. C. Y. Yang, J. Chen, T. T. Qing, X. L. Fan, W. Sun, A. von Cresce, M. S. Ding, O. Borodin, J. Vatamanu, M. A. Schroeder, N. Eidson, C. S. Wang and K. Xu, *Joule*, 2017, **1**, 122-132.
142. F. Zhang, B. Ji, X. F. Tong, M. H. Sheng, X. L. Zhang, C. S. Lee and Y. B. Tang, *Adv Mater Interfaces*, 2016, **3**, 1600605.
143. S. Komaba, W. Murata, T. Ishikawa, N. Yabuuchi, T. Ozeki, T. Nakayama, A. Ogata, K. Gotoh and K. Fujiwara, *Adv Funct Mater*, 2011, **21**, 3859-3867.
144. N. Liu, Z. D. Lu, J. Zhao, M. T. McDowell, H. W. Lee, W. T. Zhao and Y. Cui, *Nat Nanotechnol*, 2014, **9**, 187-192.
145. Y. Shi, Z. B. Yi, Y. P. Kuang, H. Y. Guo, Y. Z. Li, C. Liu and Z. G. Lu, *Chem Commun*, 2020, **56**, 11613-11616.
146. C. X. Xu and J. J. Jiang, *Rare Metals*, 2021, **40**, 243-245.
147. Z. B. Yi, Y. Liu, Y. Z. Li, L. J. Zhou, Z. Y. Wang, J. Q. Zhang, H. Cheng and Z. G. Lu, *Small*, 2020, **16**, 1905301.
148. L. J. Chen, K. M. Song, J. Shi, J. Y. Zhang, L. W. Mi, W. H. Chen, C. T. Liu and C. Y. Shen, *Sci China Mater*, 2021, **64**, 105-114.
149. Q. M. Gan, H. N. He, Y. H. Zhu, Z. Y. Wang, N. Qin, S. Gu, Z. Q. Li, W. Luo and Z. G. Lu, *Acs Nano*, 2019, **13**, 9247-9258.
150. X. Lian, Z. R. Ma, Z. H. Zhang, J. L. Yang, S. Sun, C. D. Gu, Y. Liu, H. H. Ding, J. Hu, X. Cao, J. F. Zhu, S. Z. Li and W. Chen, *Nano Res*, 2020, **13**, 3224-3229.
151. M. Favaro, J. H. Yang, S. Nappini, E. Magnano, F. M. Toma, E. J. Crumlin, J. Yano and I. D. Sharp, *J Am Chem Soc*, 2017, **139**, 8960-8970.
152. P. Munster, A. Heckmann, R. Nolle, M. Winter, K. Beltrop and T. Placke, *Batteries Supercaps*, 2019, **2**, 992-1006.
153. S. H. Kim, Y. S. Kim, W. J. Baek, S. Heo, S. Han and H. Jung, *J Power Sources*, 2018, **407**, 1-5.
154. W. Lu, J. S. Zhang, J. J. Xu, X. D. Wu and L. W. Chen, *ACS Applied Materials & Interfaces*, 2017, **9**, 19313-19318.
155. X. F. Wang, Y. J. Li and Y. S. Meng, *Joule*, 2018, **2**, 2225-2234.
156. X. F. Wang, M. H. Zhang, J. Alvarado, S. Wang, M. Sina, B. Y. Lu, J. Bouwer, W. Xu, J. Xiao, J. G. Zhang, J. Liu and Y. S. Meng, *Nano Lett*, 2017, **17**, 7606-7612.
157. Y. Z. Li, Y. B. Li, A. L. Pei, K. Yan, Y. M. Sun, C. L. Wu, L. M. Joubert, R. Chin, A. L. Koh, Y. Yu, J. Perrino, B. Butz, S. Chu and Y. Cui, *Science*, 2017, **358**, 506-510.
158. Z. Shadike, H. Lee, O. Borodin, X. Cao, X. L. Fan, X. L. Wang, R. Q. Lin, S. M. Bak, S. Ghose, K. Xu, C. S. Wang, J. Liu, J. Xiao, X. Q. Yang and E. Y. Hu, *Nat Nanotechnol*, 2021, 549–554.
159. J. Yu, C. Mu, X. Y. Qin, C. Shen, B. Y. Yan, H. G. Xue and H. Pang, *Adv Mater Interfaces*, 2017, **4**, 1700279.
160. X. Q. Shan, D. S. Charles, Y. K. Lei, R. M. Qiao, G. F. Wang, W. L. Yang, M. Feygenson, D. Su and X. W. Teng, *Nature Communications*, 2016, **7**, 13370.
161. S. Rothermel, P. Meister, G. Schmuelling, O. Fromm, H. W. Meyer, S. Nowak, M. Winter and T. Placke, *Energ Environ Sci*, 2014, **7**, 3412-3423.
162. Z. W. Zhang, J. L. Yang, W. Huang, H. S. Wang, W. J. Zhou, Y. B. Li, Y. Z. Li, J. W. Xu, W. X. Huang, W. Chiu and Y. Cui, *Matter-Us*, 2021, **4**, 302-312.
163. W. Liu, X. F. Li, D. B. Xiong, Y. C. Hao, J. W. Li, H. R. Kou, B. Yan, D. J. Li, S. G. Lu, A. Koo, K. Adair and X. L. Sun, *Nano Energy*, 2018, **44**, 111-120.
164. S. C. Jung and Y. K. Han, *J Phys Chem Lett*, 2013, **4**, 2681-2685.
165. S. Neudeck, A. Mazilkin, C. Reitz, P. Hartmann, J. Janek and T. Brezesinski, *Sci Rep-Uk*, 2019, **9**, 5328.
166. X. Chen, M. Voros, J. C. Garcia, T. T. Fister, D. B. Buchholz, J. Franklin, Y. G. Du, T. C. Droubay, Z. X. Feng, H. Iddir, L. A. Curtiss, M. J. Bedzyk and P. Fenter, *ACS Appl Energ Mater*, 2018, **1**, 2526-2535.
167. Z. X. Feng, X. Chen, L. Qiao, A. L. Lipson, T. T. Fister, L. Zeng, C. Kim, T. H. Yi, N. Sa, D. L. Proffit, A. K. Burrell, J. Cabana, B. J. Ingram, M. D. Biegalski, M. J. Bedzyk and P. Fenter, *ACS Applied Materials & Interfaces*, 2015, **7**, 28438-28443.
168. Z. X. Feng, X. Chen, T. T. Fister, M. J. Bedzyk and P. Fenter, *J Appl Phys*, 2016, **120**, 015307.
169. X. F. He, Y. Z. Zhu and Y. F. Mo, *Nature Communications*, 2017, **8**, 15893.
170. Y. H. Zhang, J. F. Qian, W. Xu, S. M. Russell, X. L. Chen, E. Nasybulin, P. Bhattacharya, M. H. Engelhard, D. H. Mei, R. G. Cao, F. Ding, A. V. Cresce, K. Xu and J. G. Zhang, *Nano Lett*, 2014, **14**, 6889-6896.
171. Y. Li, D. X. Cao, W. Arnold, Y. Ren, C. Liu, J. B. Jasinski, T.

Druffel, Y. Cao, H. L. Zhu and H. Wang, *Energy Storage Mater*, 2020, **31**, 344-351.
172. Z. J. Ju, J. W. Nai, Y. Wang, T. F. Liu, J. H. Zheng, H. D. Yuan, O. W. Sheng, C. B. Jin, W. K. Zhang, Z. Jin, H. Tian, Y. J. Liu and X. Y. Tao, *Nature Communications*, 2020, **11**, 488.
173. T. Y. Wang, Y. B. Li, J. Q. Zhang, K. Yan, P. Jaumaux, J. Yang, C. Y. Wang, D. Shanmukaraj, B. Sun, M. Armand, Y. Cui and G. X. Wang, *Nature Communications*, 2020, **11**, 5429.
174. X. Y. Zhang, A. X. Wang, X. J. Liu and J. Y. Luo, *Accounts Chem Res*, 2019, **52**, 3223-3232.
175. J. M. He, C. Yang, X. Yang, L. L. Liu, J. H. Li, Q. Liu, L. Peng, X. R. Liu and M. N. Qu, *Appl Surf Sci*, 2020, **532**.
176. H. Guzman, F. Zammillo, D. Roldan, C. Galletti, N. Russo and S. Hernandez, *Catalysts*, 2021, **11**.
177. H. Cheng, W. Yuan and K. Scott, *J Power Sources*, 2008, **183**, 678-681.
178. Z. J. Liang, Q. L. Zou, Y. Wang and Y. C. Lu, *Small Methods*, 2017, **1**.
179. E. Murawski, N. Kananizadeh, S. Lindsay, A. M. Rao and S. C. Popat, *J Power Sources*, 2021, **481**.
180. I. Asano, Y. Hamano, S. Tsujimura, O. Shirai and K. Kano, *Electrochemistry*, 2012, **80**, 324-326.
181. V. Briega-Martos, G. A. B. Mello, R. M. Aran-Ais, V. Climent, E. Herrero and J. M. Feliu, *J Electrochem Soc*, 2018, **165**, J3045-J3051.
182. V. Briega-Martos, E. Herrero and J. M. Feliu, *Electrochim Acta*, 2017, **241**, 497-509.
183. S. Rojas-Carbonell, K. Artyushkova, A. Serov, C. Santoro, I. Matanovic and P. Atanassov, *Acs Catalysis*, 2018, **8**, 3041-3053.
184. A. Schumpe, I. Adler and W. D. Deckwer, *Biotechnol Bioeng*, 1978, **20**, 145-150.
185. E. Narita, F. Lawson and K. N. Han, *Hydrometallurgy*, 1983, **10**, 21-37.
186. W. McKee, S. Rawal and Y. Xu, *Abstr Pap Am Chem S*, 2016, **252**.
187. L. J. Su, L. Y. Liu, B. Liu, J. N. Meng and X. B. Yan, *Iscience*, 2020, **23**.
188. w. Xing, G. Yin and J. Zhang, *Rotating Electrode Methods and Oxygen Reduction Electrocatalysts*, Elsevier Science, 2014.
189. F. S. Gittleson, R. E. Jones, D. K. Ward and M. E. Foster, *Energ Environ Sci*, 2017, **10**, 1167-1179.
190. Y. Kanzaki, K. Tokuda and S. Bruckenstein, *J Electrochem Soc*, 2014, **161**, H770-H779.
191. Y. H. Shih, G. V. Sagar and S. D. Lin, *J Phys Chem C*, 2008, **112**, 123-130.
192. P. Kubicek, *Collect Czech Chem C*, 1978, **43**, 535-544.
193. S. C. Xu, Y. Kim, D. Higgins, M. Yusuf, T. F. Jaramillo and F. B. Prinz, *Electrochim Acta*, 2017, **255**, 99-108.
194. X. Y. Mao, C. Lin, G. W. Graham and R. J. Gorte, *ACS Catalysis*, 2020, **10**, 8840-8849.
195. H. Kawasoko, T. Shirasawa, S. Shiraki, T. Suzuki, S. Kobayashi, K. Nishio, R. Shimizu and T. Hitosugi, *ACS Appl Energ Mater*, 2020, **3**, 1358-1363.
196. S. Shiraki, T. Shirasawa, T. Suzuki, H. Kawasoko, R. Shimizu and T. Hitosugi, *ACS Applied Materials & Interfaces*, 2018, **10**, 41732-41737.
197. H. Kawasoko, S. Shiraki, T. Suzuki, R. Shimizu and T. Hitosugi, *ACS Applied Materials & Interfaces*, 2018, **10**, 27498-27502.
198. Y. He, M. Gu, H. Y. Xiao, L. L. Luo, Y. Y. Shao, F. Gao, Y. G. Du, S. X. Mao and C. M. Wang, *Angew Chem Int Edit*, 2016, **55**, 6244-6247.
199. Y. Z. Zhu, X. F. He and Y. F. Mo, *Journal of Materials Chemistry A*, 2016, **4**, 3253-3266.
200. J. W. Ju, J. Ma, Y. T. Wang, Y. Y. Cui, P. X. Han and G. L. Cui, *Energy Storage Mater*, 2019, **20**, 269-290.
201. N. C. Rosero-Navarro, R. Kajiura, A. Miura and K. Tadanaga, *ACS Appl Energ Mater*, 2020, **3**, 11260-11268.
202. F. Lv, Z. Y. Wang, L. Y. Shi, J. F. Zhu, K. Edstrom, J. Mindemark and S. Yuan, *J Power Sources*, 2019, **441**, 227175.
203. D. P. Clark and R. E. Meredith, *Electrochem Technol*, 1967, **5**, 446-&.
204. F. J. Q. Cortes, J. A. Lewis, J. Tippens, T. S. Marchese and M. T. McDowell, *J Electrochem Soc*, 2019, **167**, 050502.
205. J. Y. Yang, Z. H. Gao, T. Ferber, H. F. Zhang, C. Guhl, L. T. Yang, Y. Y. Li, Z. Deng, P. R. Liu, C. W. Cheng, R. C. Che, W. Jaegermann, R. Hausbrand and Y. H. Huang, *Journal of Materials Chemistry A*, 2020, **8**, 7828-7835.
206. H. H. Xu, P. H. Chien, J. J. Shi, Y. T. Li, N. Wu, Y. Y. Liu, Y. Y. Hu and J. B. Goodenough, *P Natl Acad Sci USA*, 2019, **116**, 18815-18821.
207. W. B. Zhang, T. Leichtweiss, S. P. Culver, R. Koerver, D. Das, D. A. Weber, W. G. Zeier and J. Janek, *ACS Applied Materials & Interfaces*, 2017, **9**, 35888-35896.
208. X. G. Hao, Q. Zhao, S. M. Su, S. Q. Zhang, J. B. Ma, L. Shen, Q. P. Yu, L. Zhao, Y. Liu, F. Y. Kang and Y. B. He, *Adv Energy Mater*, 2019, **9**, 1901604.
209. B. B. Wu, S. Y. Wang, J. Lochala, D. Desrochers, B. Liu, W. Q. Zhang, J. H. Yang and J. Xiao, *Energ Environ Sci*, 2018, **11**, 1803-1810.
210. T. An, H. H. Jia, L. F. Peng and J. Xie, *ACS Applied Materials & Interfaces*, 2020, **12**, 20563-20569.
211. D. X. Cao, X. Sun, Q. Li, A. Natan, P. Y. Xiang and H. L. Zhu, *Matter-Us*, 2020, **3**, 57-94.
212. H. Liu, X. B. Cheng, J. Q. Huang, H. Yuan, Y. Lu, C. Yan, G. L. Zhu, R. Xu, C. Z. Zhao, L. P. Hou, C. X. He, S. Kaskel and Q. Zhang, *ACS Energy Letters*, 2020, **5**, 833-843.
213. X. Zhang, S. Wang, C. J. Xue, C. Z. Xin, Y. H. Lin, Y. Shen, L. L. Li and C. W. Nan, *Advanced Materials*, 2019, **31**, 1806082.
214. G. M. Hou, X. X. Ma, Q. D. Sun, Q. Ai, X. Y. Xu, L. N. Chen, D. P. Li, J. H. Chen, H. Zhong, Y. Li, Z. B. Xu, P. C. Si, J. K. Feng, L. Zhang, F. Ding and L. J. Ci, *ACS Applied Materials & Interfaces*, 2018, **10**, 18610-18618.
215. S. F. Wang, H. H. Xu, W. D. Li, A. Dolocan and A. Manthiram, *J Am Chem Soc*, 2018, **140**, 250-257.
216. Q. Zhao, P. Y. Chen, S. K. Li, X. T. Liu and L. A. Archer, *Journal of Materials Chemistry A*, 2019, **7**, 7823-7830.
217. S. F. Lou, F. Zhang, C. K. Fu, M. Chen, Y. L. Ma, G. P. Yin and J. J. Wang, *Advanced Materials*, 2020, 2000721.
218. M. Le Granvalet-Mancini, T. Hanrath and D. Teeters, *Solid State Ionics*, 2000, **135**, 283-290.
219. N. L. Wu, Y. T. Weng, F. S. Li, N. H. Yang, C. L. Kuo and D. S. Li, *Prog Nat Sci-Mater*, 2015, **25**, 563-571.
220. D. C. Zhang, L. Zhang, K. Yang, H. Q. Wang, C. Yu, D. Xu, B. Xu and L. M. Wang, *ACS Applied Materials & Interfaces*, 2017, **9**, 36886-36896.
221. N. W. Li, Y. X. Yin, C. P. Yang and Y. G. Guo, *Advanced Materials*, 2016, **28**, 1853-1858.
222. K. Thanner, A. Varzi, D. Buchholz, S. J. Sedlmaier and S.

Passerini, *ACS Applied Materials & Interfaces*, 2020, **12**, 32851-32862.
223. S. Wang, R. Fang, Y. Li, Y. Liu, C. Xin, F. H. Richter and C.-W. Nan, *Journal of Materiomics*, 2021, **7**, 209-218.
224. Y. F. Mo, S. P. Ong and G. Ceder, *Chemistry of Materials*, 2012, **24**, 15-17.
225. T. Watanabe, Y. Aihara, S. Fujiki, S. Ito and T. Yamada, *Abstr Pap Am Chem S*, 2016, **252**.
226. M. R. Busche, D. A. Weber, Y. Schneider, C. Dietrich, S. Wenzel, T. Leichtweiss, D. Schroder, W. B. Zhang, H. Weigand, D. Walter, S. J. Sedlmaier, D. Houtarde, L. F. Nazar and J. Janek, *Chemistry of Materials*, 2016, **28**, 6152-6165.
227. Y. Z. Zhu, X. F. He and Y. F. Mo, *ACS Applied Materials & Interfaces*, 2015, **7**, 23685-23693.
228. T. Hakari, M. Nagao, A. Hayashi and M. Tatsumisago, *J Power Sources*, 2015, **293**, 721-725.
229. S. Wenzel, T. Leichtweiss, D. Kruger, J. Sann and J. Janek, *Solid State Ionics*, 2015, **278**, 98-105.
230. C. Z. Sun, Y. D. Ruan, W. P. Zha, W. W. Li, M. L. Cai and Z. Y. Wen, *Mater Horiz*, 2020, **7**, 1667-1696.
231. M. Nagao, A. Hayashi and M. Tatsumisago, *Electrochemistry*, 2012, **80**, 734-736.
232. T. Ates, M. Keller, J. Kulisch, T. Adermann and S. Passerini, *Energy Storage Mater*, 2019, **17**, 204-210.
233. F. J. Simon, M. Hanauer, A. Henss, F. H. Richter and J. Janek, *ACS Applied Materials & Interfaces*, 2019, **11**, 42186-42196.
234. Y. H. Xiao, Y. Wang, S. H. Bo, J. C. Kim, L. J. Miara and G. Ceder, *Nat Rev Mater*, 2020, 105–126.
235. Z. J. Bi, N. Zhao, L. N. Ma, Z. Q. Fu, F. F. Xu, C. S. Wang and X. X. Guo, *Chem Eng J*, 2020, **387**, 124089.
236. K. H. Nie, Y. S. Hong, J. L. Qiu, Q. H. Li, X. Q. Yu, H. Li and L. Q. Chen, *Front Chem*, 2018, **6**, 00616.
237. A. Schwobel, W. Jaegermann and R. Hausbrand, *Solid State Ionics*, 2016, **288**, 224-228.
238. J. Song, S. Jacke, G. Cherkashinin, S. Schmid, Q. F. Dong, R. Hausbrand and W. Jaegermann, *Electrochem Solid St*, 2011, **14**, A189-A191.
239. M. F. Groh, M. J. Sullivan, M. W. Gaultois, O. Pecher, K. J. Griffith and C. P. Grey, *Chemistry of Materials*, 2018, **30**, 5886-5895.
240. J. Auvergniot, A. Cassel, J. B. Ledeuil, V. Viallet, V. Seznec and R. Dedryvere, *Chemistry of Materials*, 2017, **29**, 3883-3890.
241. A. Sakuda, A. Hayashi and M. Tatsumisago, *Chemistry of Materials*, 2010, **22**, 949-956.
242. K. H. Kim, Y. Iriyama, K. Yamamoto, S. Kumazaki, T. Asaka, K. Tanabe, C. A. J. Fisher, T. Hirayama, R. Murugan and Z. Ogumi, *J Power Sources*, 2011, **196**, 764-767.
243. Z. Z. Tong, S. B. Wang, Y. K. Liao, S. F. Hu and R. S. Liu, *ACS Applied Materials & Interfaces*, 2020, **12**, 47181-47196.
244. K. Yoshima, Y. Harada and N. Takami, *J Power Sources*, 2016, **302**, 283-290.
245. C. W. Wang, F. C. Ren, Y. Zhou, P. F. Yan, X. D. Zhou, S. J. Zhang, W. Liu, W. D. Zhang, M. H. Zou, L. Y. Zeng, X. Y. Yao, L. Huang, J. T. Li and S. G. Sun, *Energ Environ Sci*, 2021, **14**, 437-450.
246. H. Wang, M. Yu, Y. Wang, Z. X. Feng, Y. Q. Wang, X. J. Lu, J. L. Zhu, Y. Ren and C. D. Liang, *J Power Sources*, 2018, **401**, 111-116.
247. M. Lucero, S. Qiu and Z. Feng, *Carbon Energy*, 2021, 563–580.